remote sensing

MDPI

Article

Identifying Land-Use Related Potential Disaster Risk Drivers in the Ayeyarwady Delta (Myanmar) during the Last 50 Years (1974–2021) Using a Hybrid Ensemble Learning Model

Anissa Vogel [1,*], Katharina Seeger [1], Dominik Brill [1], Helmut Brückner [1], Khin Khin Soe [2], Nay Win Oo [3], Nilar Aung [4], Zin Nwe Myint [2] and Frauke Kraas [1]

[1] Institute of Geography, University of Cologne, Albertus-Magnus-Platz, 50923 Cologne, Germany; k.seeger@uni-koeln.de (K.S.); brilld@uni-koeln.de (D.B.); h.brueckner@uni-koeln.de (H.B.); f.kraas@uni-koeln.de (F.K.)
[2] Department of Geography, University of Yangon, University Avenue Road, Kamayut Township, Yangon 11041, Myanmar; khinkhinsoe@uy.edu.mm (K.K.S.); zinnwemyint@uy.edu.mm (Z.N.M.)
[3] East Yangon University, East Yangon University Road, Thanlyin Township, Thanlyin 11291, Myanmar; eyuthanlyin@eyu.edu.mm
[4] Taunggoke University, Taunggoke, Myanmar; taunggokeuni@gmail.com
* Correspondence: a.vogel@uni-koeln.de

Abstract: Land-use and land-cover change (LULCC) dynamics significantly impact deltas, which are among the world's most valuable but also vulnerable habitats. Non-risk-oriented LULCCs can act as disaster risk drivers by increasing levels of exposure and vulnerability or by reducing capacity. Making thematically detailed long-term LULCC data available is crucial to improving understanding of those dynamics interlinked at different spatiotemporal scales. For the Ayeyarwady Delta, one of the least studied mega-deltas, such comprehensive information is still lacking. This study used 50 Landsat and Sentinel-1A images spanning five decades from 1974 to 2021 in five-year intervals. A hybrid ensemble model consisting of six machine-learning classifiers was employed to generate land-cover maps from the images, achieving accuracies of about 90%. The major identified potential risk-relevant LULCC dynamics include urban growth towards low-lying areas, mangrove deforestation, and the expansion of irrigated agricultural areas and cultivated aquatic surfaces. The novel area-wide LULCC products achieved through the analyses provide a basis to support future risk-sensitive development decisions and can be used for regionally adapted disaster risk management plans and models. Developed with freely available data and open-source software, they hold great potential to increase research activity in the Ayeyarwady Delta and will be shared upon request.

Keywords: Ayeyarwady Delta; Myanmar; mega-delta; land cover classification; ensemble learning; Landsat; Sentinel; disaster risk drivers

Citation: Vogel, A.; Seeger, K.; Brill, D.; Brückner, H.; Khin Khin Soe; Nay Win Oo; Nilar Aung; Zin Nwe Myint; Kraas, F. Identifying Land-Use Related Potential Disaster Risk Drivers in the Ayeyarwady Delta (Myanmar) during the Last 50 Years (1974–2021) Using a Hybrid Ensemble Learning Model. *Remote Sens.* **2022**, *14*, 3568. https://doi.org/10.3390/rs14153568

Academic Editors: Lucie Kupková and Markéta Potůčková

Received: 17 June 2022
Accepted: 21 July 2022
Published: 25 July 2022

1. Introduction

During the Anthropocene, land use dynamics have become a global force that crucially affect the Earth system [1–3]. Land-use/land-cover change (LULCC) has altered about a third of the global land area in just six decades since 1960, with drastic consequences accumulating particularly in so-called developing nations [4].

Various studies have found a correlation between consequences of LULCC, vulnerability, and the impact of hazards, turning them into disasters [5–10]. This connection can be part of what is termed a "new era of risk" [11] (p. 3), created by the conjunction of a security and environmental crisis, where the first will not be solved without addressing environmental degradation [11]. Therefore, disasters are "long-term processes of maldevelopment" [9] (p. 7), indicating unsustainable development processes [12]. Underlying disaster risk drivers (or disaster risk factors) are defined by the United Nations Office for

Disaster Risk Reduction (UNDRR) as "processes or conditions, often development-related, that influence the level of disaster risk by increasing levels of exposure and vulnerability or reducing capacity" [13] (para. 1). According to the Global Assessment Report on Disaster Risk Reduction [14] and the Sendai Framework [15], underlying disaster risk drivers include demographic pressures, poverty and inequality, environmental degradation and the decline of ecosystem services, climate change, weak governance structures, and "the lack of disaster risk considerations in land management and environmental and natural resource management" [13] (para. 2). Non-risk-oriented LULCC dynamics have the potential to trigger, increase, or even create disaster risks [16].

Representing key challenges of global change, potential disaster risk drivers are progressing faster and more intensely in deltaic areas, the "hotspots in the Anthropocene transition" [17] (p. 2), which have been exposed to more than 7000 years of resource exploitation [17,18]. A global empirical typology of anthropogenic drivers of environmental change in deltas can be found in [19]. Deltas are among the most economical and ecologically valuable environments worldwide [20,21]. With a population density eight times the global average [18] and an expected population of more than a billion people by 2060 [22], they are, at least on a global scale, key settlement areas for the majority of the population of most coastal countries [23]. Located on the interface between land and water with a mostly flat topography, deltaic areas combine numerous locational advantages such as abundant riverine and marine resources, fertile alluvial soils, various ecosystem services, and high biodiversity [24]. Deltas and their multiple transportation possibilities are often crucial for the resource-based economy and food security of entire nations [24], and they are essential places of national socio-economic and urban development, often of capital and primate (mega)cities [23,25,26]. At the same time, deltas are highly vulnerable ecosystems, facing increasing risk due to global sea-level rise, unsustainable regional water management and human activities, land subsidence, climate change, and various ocean-born threats [24,27].

As some of these processes are characterised by time-lag effects (e.g., in the case of deltaic subsidence [28,29]) and can act on longer time scales, detailed knowledge of long-term spatio-temporal development processes constituting LULCC dynamics is required to understand potential disaster risks and their underlying drivers, and thus to set the course for "risk-sensitive development decisions" [7] (p. 1). However, while many deltas are well studied, the Ayeyarwady Delta in Myanmar remains one of the least studied mega-deltas in the world, despite its outstanding importance for the country and region as part of one of the world's major tropical river systems [30–32]. The political situation and reduced accessibility of Myanmar have made access to the delta difficult and led to several research gaps [33–37].

Against this background, remote sensing is one of the most important technologies available for the long-term analysis of land surface dynamics, especially in data-poor and difficult to access regions [38]. Technological advances have made possible what is called a "new era of land cover analysis" [39] (p. 4254), allowing for a cost- and time-efficient, spatially extensive, multi-temporal, and high-frequency analysis of LULCC dynamics worldwide. Furthermore, remote sensing is also particularly suitable as a primary support tool for disaster risk management to investigate, monitor, and assess the spatially and temporally highly dynamic disaster risk processes [40,41]. The practical relevance is demonstrated, for example, by the Sentinel Asia programme for disaster management support in the Asia-Pacific region, a programme launched in 2005 by the Asia-Pacific Regional Space Agency Forum [41].

Several recent approaches have successfully utilized remote sensing methods in the Ayeyarwady Delta, albeit with a narrow thematic, spatial, or temporal focus. Using four Landsat images from between 1978 and 2011, Webb et al. [36] identified the expansion of agricultural land as the main driver of deforestation in the delta. Torbick et al. [42] analysed the rice-based agriculture in Myanmar with a dense, intra-annual time series of Sentinel-1, Landsat, and PALSAR-2 imagery between 2015 and 2016. More specifically, Sakai et al. [43] monitored the seasonality of saline intrusion in the delta for 2018 and changes in the rice

cropping system between 1981 and 2020 using Sentinel-2 imagery and a global NDVI dataset, respectively. A coarse environmental change detection using four Landsat scenes from between 2000 and 2017 was undertaken by Soe Soe Khaing et al. [44]. In addition, a few recent studies has given a more comprehensive overview of the Ayeyarwady Delta, focusing on the geomorphological evolution of the delta and the river system [30–32,45,46]. What is still lacking, and thus hindering informed decisions on risk-sensitive development, is a comprehensive analysis of long-term LULCC dynamics and their relationship to potential disaster risk at a high spatio-temporal resolution for the entire Ayeyarwady Delta.

While international experts and decision makers are calling for "freely available, reliable, quantitative scientific information to further improve knowledge and understanding of river delta environments" [24] (p. 2), the acquisition of that information remains challenging (for details, see [24]). Covering large areas, the availability of long-term and cloud-free images is often limited and costly. While global datasets neglect local diversity, and visual interpretation based on expert knowledge is time-consuming and prone to errors, analyses based on simple, automated methods are made difficult by the extreme spectral heterogeneity of deltaic areas [24,47,48]. In this context, multiple classifier systems or classifier ensembles combining complementary pattern information are considered to have great potential to improve the accuracy and efficiency of complex classifications [49,50].

Hence, the aim of this study is to develop an efficient framework providing a holistic long-term analysis of LULCC dynamics and related potential disaster risk drivers in the entire Ayeyarwady Delta of Myanmar, thus addressing the existing research gap. The objectives are (1) establishing a hybrid ensemble classification using six different machine-learning algorithms, combining optical Landsat data, Sentinel-1A radar data, and various spectral indices, for dense five-year intervals between 1974 and 2021; (2) systematically assessing thematically detailed LULCC dynamics; and (3) identifying potential disaster risk drivers based on the global UNDRR frameworks and specified by the LULCC analysis as a basis for supporting future risk-sensitive development decisions in the delta.

2. Materials and Methods

2.1. Study Area

The Ayeyarwady River originates in Myitsone in the south-eastern Himalayan Mountains from the confluence of the N'mai Hka, rising from the Languela glacier in the Tila massif sourced north of Puta-O, and the Mali Hka, sourced west of it in northern Kachin State [51–53]. Consisting of 415,700 km^2 [53], the river catchment covers about 60% of Myanmar's territory, concentrating the population and connecting leading cities and economic centres [54]. The Ayeyarwady River meanders over 2010 km [52] from Myitsone via the Myitkyina plains through the Central Dry Zone around Mandalay, passes the historic centres of Bagan and Sri Ksetra (today Pyay) to Hinthada and Pathein towards the Andaman Sea. There, the wedge-shaped Ayeyarwady Delta was formed 7000–8000 years ago [45] with the apex located about 90 km north of Hinthada [46], forming, together with the coastal deposits of the Sittaung River in the east, the eleventh largest delta in the world [31,45,46]. This study uses a definition of the delta based on that from Tessler et al. [27], covering an area about 40,000 km^2 (see Figure 1).

Despite large-scale environmental transformations, the Ayeyarwady River is one of the last rivers in Southeast Asia with relatively intact natural functions and ranks among the largest rivers in the world with respect to sediment discharge [32,55,56]. Since the sediment loads of Chinese rivers have declined, sediment discharges of 364 $\pm$ 60 Mt/year reported for the Ayeyarwady River make it the third largest sediment supplier in the global sediment budget [55]. While the same authors estimate annual water discharges of 422 $\pm$ 48 to 440 $\pm$ 41 km^3/year [55], Furuichi et al. [57] have documented a significant decrease of discharge of 379 $\pm$ 47 km^3/year for the 20th century. Overall, the system has remained nearly stable for the last ~150 years, with a landward movement of 0.34 km/century since 1925 [58]. Since 1974, changes along the delta coast have averaged 10.4 m/year [46], with

erosion mainly in the western part (on average −4.7 m/year) and aggradation mainly in the eastern part of the delta (on average 21.4 m/year).

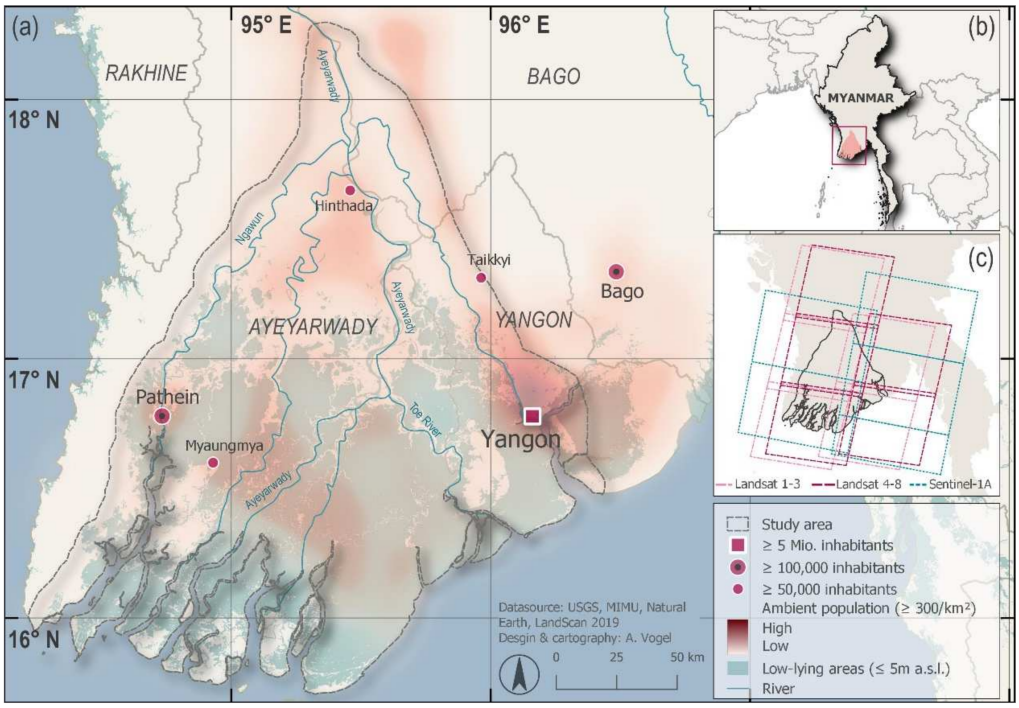

Figure 1. Location of the study area (**a**,**b**) and extents of utilized Landsat and Sentinel scenes (**c**).

The Ayeyarwady Delta is a mud–silt, tide-dominated system with a mean tidal range of 4.2 m and a shoreline of 450 km with nine mouths, comprising five major and many smaller distributaries [31,45,53]. The climate of the delta is determined by the Indian Monsoon with hot and humid months in the rainy season from May to October and relatively cool and dry months from December to March [59,60]. The mean annual rainfall in the delta ranges from 2000 to 3000 mm, while the area is prone to suffer from tropical cyclones, flooding, and droughts [59,61–63]. The Ayeyarwady basin and delta are among the most biologically diverse regions in the world, hosting 89 Key Biodiversity Area sites [64,65]. The socio-economic advantages—first and foremost in terms of agriculture, aquaculture, and industry—provided by the Ayeyarwady Delta are of outstanding relevance for Myanmar's future development [31,37,61]. The delta is already home to about 26% of the population of Myanmar (estimate based on the census 2014 [66]), including the megacity Yangon [67,68] and numerous regional and smaller cities and towns within the urbanised delta triangle of Yangon, Pathein, and Pyay [54]. Being transformed to the world's largest exporter of rice under British colonialization [33], the delta is among the important rice-producing areas of Southeast Asia and constitutes the most important agricultural region in Myanmar [69], with significant concentrations of aquaculture [70,71].

The increasing amount of anthropogenic pressure is challenging the environmental stability of the delta system [31,45,46]. In the literature, the Ayeyarwady Delta has been classified as "in peril" due to "reduction in aggradation plus accelerated compaction overwhelming rates of global sea-level rise" [72] (p. 684), increasing the potential exposure to hazardous events and leading to possible creation of risk in the future [27].

2.2. Data and Preprocessing

To analyse the LULCC dynamics in the Ayeyarwady Delta and assess their impact as potential disaster risk drivers, a hybrid ensemble learning model was established. The workflow for the generation of this hybrid ensemble learning model is shown in Figure 2.

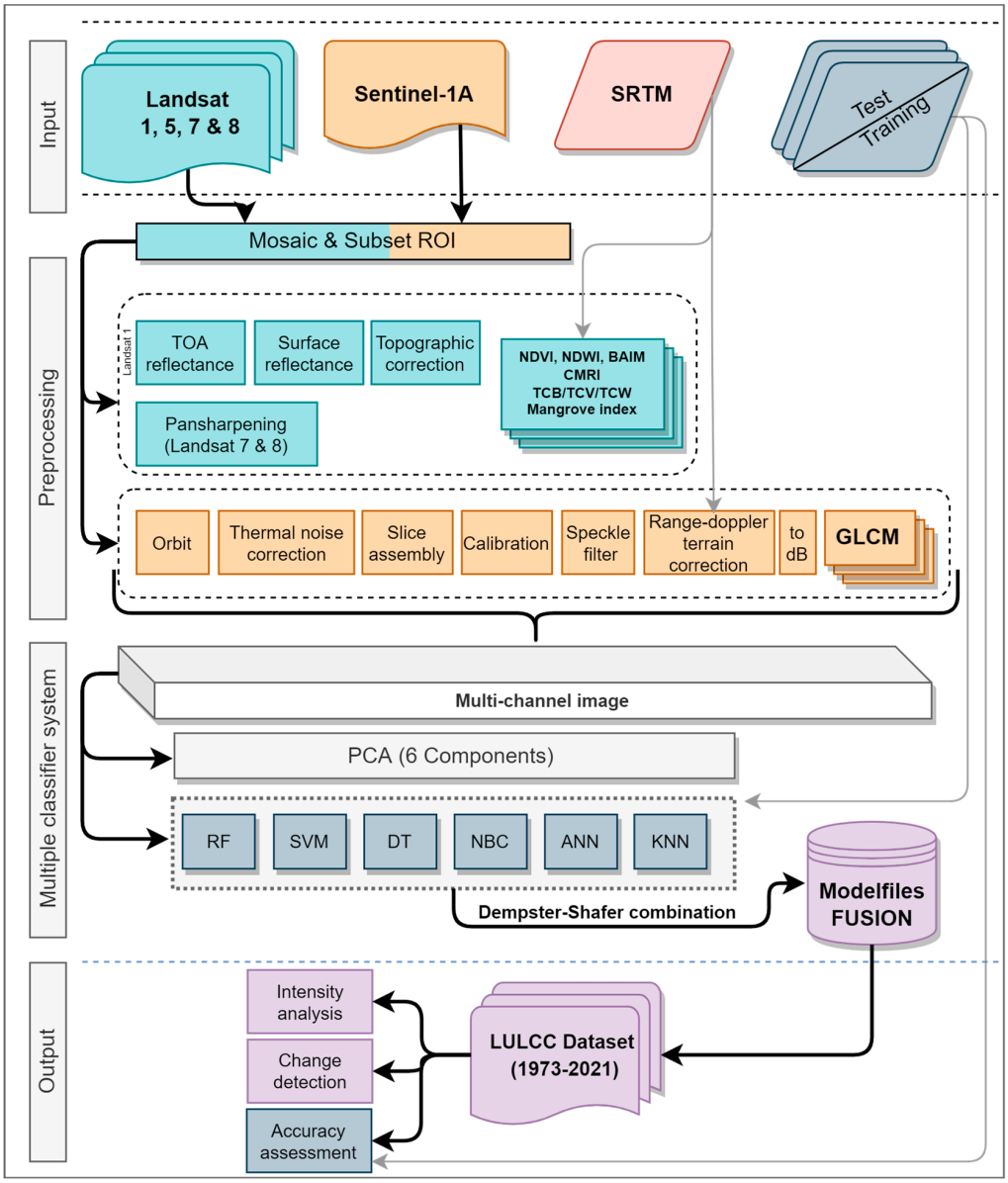

Figure 2. Overall processing workflow for the generation of the hybrid ensemble learning model including pre- and post-processing.

Landsat satellite imagery was used as the main data source for the study to establish a consistent, long-term time series covering a 48-year time period (1973–2021). Having a medium-resolution of 30 m (60 m for Landsat 1), Landsat data is particularly suitable for analysing large scale LULCC dynamics with a high degree of spectral heterogeneity, which is common in complex delta regions [24,73]. To cover the entire delta area, five intersection image frames in two different paths were used (see Figure 1c). To ensure the highest possible image quality, only cloud-free images (0% cloud coverage) acquired as close to each other as possible during the dry season from December to March were considered. Therefore, 40 Landsat images, including the baseline date 1973/1974, were used in a nearly five-year-interval timeframe spanning from 1990 to 2021: Landsat-1 MSS (1973/1974; hereafter 1974), Landsat-5 TM (1990, 1995, 2005, 2010), Landsat-7 ETM+ (2001), and Landsat-8 OLI (2015–2021). Additionally, five Sentinel-1A images were used for each of the most recent years, 2015 and 2021. As an active sensing system, the Sentinel-1A C-band Synthetic Aperture Radar (SAR) instrument at 5.405 GHz provides comparative advantages

such as all-weather capability and complementary sensitivity to soil moisture and water content. For a complete overview of the 50 datasets used, see Table 1.

Table 1. Remote Sensing data used in this study with corresponding time intervals.

Time	No.	Date	Scenes	Sensor	Ground Res.	Bands
1	1–2	1973/12/18	2	Landsat 1 MSS	79 m × 79 m [1]	4
	3–5	1974/02/11	3	Landsat 1 MSS	79 m × 79 m [1]	4
2	6–8	1990/01/11	3	Landsat 5 TM	30 m × 30 m	7
	9–10	1990/02/05	2	Landsat 5 TM	30 m × 30 m	7
3	11–13	1995/02/10	3	Landsat 5 TM	30 m × 30 m	7
	14–15	1995/02/19	2	Landsat 5 TM	30 m × 30 m	7
4	16–17	2001/02/27	2	Landsat 7 ETM+	30 m × 30 m	8
	18–20	2001/03/06	3	Landsat 7 ETM+	30 m × 30 m	8
5	21–23	2005/02/05	3	Landsat 5 TM	30 m × 30 m	7
	24–25	2005/02/14	2	Landsat 5 TM	30 m × 30 m	7
6	26–28	2010/02/03	3	Landsat 5 TM	30 m × 30 m	7
	29–30	2010/02/12	2	Landsat 5 TM	30 m × 30 m	7
7	31–33	2015/02/17	3	Landsat 8 OLI	30 m × 30 m	11
	34–35	2015/02/26	2	Landsat 8 OLI	30 m × 30 m	11
	36–37	2015/02/09	2	Sentinel-1A	20 m × 20 m	VV, VH
	38–40	2015/02/28	3	Sentinel-1A	20 m × 20 m	VV, VH
8	41–42	2021/02/15	2	Landsat 8 OLI	30 m × 30 m	11
	43–45	2021/02/01	3	Landsat 8 OLI	30 m × 30 m	11
	46–47	2021/02/01	2	Sentinel-1A	20 m × 20 m	VV, VH
	48–50	2021/01/27	3	Sentinel-1A	20 m × 20 m	VV, VH
1–8	51	SRTM 1 Arc-Second Global			(30 m)	

[1] delivered data resampled to 60 m pixel size.

All Landsat data were downloaded via the open access USGS Earth explorer. The Landsat-8, Landsat-7, and Landsat-5 images were provided as Level-2 surface reflectance science products.

Pre-processing was conducted using the open source Orfeo ToolBox (OTB 7.4.0). As Landsat-7 and Landsat-8 have a panchromatic channel, a statistical pan-sharpening algorithm was used to increase the spatial resolution of the 30 m multispectral bands to 15 m, which improved the classification accuracy significantly [74,75]. Additional spectral information increased the separability of classes and decreased the sensitivity to differences between the single satellite images common in large area mosaics and therefore also enhanced the classification accuracy [42,73,76]. Hence, the well-established Normalized Difference Vegetation Index (NDVI) [77], the Normalized Difference Water Index (NDWI) [78], the modified Burned Area Index (BAIM) [79], and—more specific for inland water and pond classes—the Normalized Difference Turbidity Index (NDTI) [80] were calculated for the Landsat images. As the discrimination of mangroves from non-mangrove vegetation posed a special challenge in the study area, the Combined Mangrove Recognition Index [81] was calculated for the Landsat data and combined with a topographic mask based on the NASA SRTM Digital Elevation Modell (30 m) to exclude areas with an elevation higher than 39 m where mangroves in Myanmar do not naturally occur [82].

The Sentinel-1A images were obtained from the Copernicus Open Access Hub as dual-polarized (VV + VH) Level-1 Ground Range Detected (GRD) products in the Interferometric Wide Swath (IW) Mode and were further pre-processed using the ESA open source toolbox SNAP (8.0.0). The Level-1 slice products were seamlessly combined into assembled products in line with the two unique Sentinel orbits covering the study area. Thermal noise was removed, and the annotated orbit information was updated using precise orbit state vectors before the data were converted to sigma nought. A gamma map filter

with a 3 × 3 kernel size was applied to all images to reduce the granular noise. A Range Doppler Terrain Correction using the NASA SRTM 1 sec HGT was applied, and all image values were converted to the dB scale. To increase the texture description and separability of different land-use/land-cover (LULC) types in the complex wetland landscape of the delta, seven Gray-Level-Co-Occurrence Matrix (GLCM) texture variables (homogeneity, energy, maximum probability, entropy, and mean) were calculated [83,84]. The Landsat- and Sentinel-1A images were co-registered and stacked using SNAP and utilized together with the indices and GLCM variables. The dimensionality of the multi-channel images was reduced to six components using principal component analysis (PCA), providing a balanced tradeoff between accuracy and processing efficiency. The results were used as input for the hybrid ensemble classifier model.

2.3. Hybrid Ensemble Model and Change Detection

A specific classification scheme was developed based on existing land use research, expert knowledge about the area, and high-resolution Google Earth imagery with respect to the medium-resolution of the utilized Landsat data, resulting in 10 major LULC classes (see Table 2).

Table 2. Classification scheme including major landscape characteristics.

ID	LULC Classes	Description
1	Urban and built-up areas	Sparsely to densely built-up areas, including industrial, commercial, and transportation units as well as urban green areas
2	Shrubland	Sparsely vegetated areas, including mosaics of agricultural and natural vegetation in different transition stages
3	Forest	Densely vegetated broadleaf forest areas (closed)
4	Mangroves	Coastal saline and brackish vegetation
5	Dry crops	Non-irrigated farmland (dry-season bare fields), including fallow land and burnt areas
6	Irrigated crops	Predominantly irrigated farmland (dry-season grown fields), including early growing and different irrigation stages
7	Aquaculture	Cultivated water ponds for inland aquaculture production (mainly fish and shrimps)
8	Brine ponds	Shallow salt-water ponds for mineral extraction (mainly salt)
9	Water	Inland or marine water courses and water bodies, including water reservoirs
10	Sediment plains	Non-vegetated sediment deposit areas, including tidal flats and sand banks

Training polygons for the classifier were created using Google Earth high-resolution imagery and complementary aerial photography. The training samples were generated randomly stratified to represent the different LULC classes proportional to their area, which improved the classification results [85]. The training samples were digitized across the entire study area to capture different landscape conditions and different spectral and illumination characteristics across the mosaics. As a result, representative datasets were available, with training samples between 50,000 and 100,000 pixel per class, for every classified image and each of the two Landsat paths covering the study area.

The pixel-based multiple classifier system was designed and performed using the open source Orfeo ToolBox (OTB 7.4.0). First, a pool of classifiers was created from six machine learning algorithms. Since the accuracy of the ensemble strongly depends on the diversity of the classifiers [49], a hybrid approach with different classifiers with different specialties and accuracies was chosen, consisting of a Random Forest (RF), Decision Tree (DT), Support Vector Machine (SVM), k-Nearest Neighbour (KNN), Artificial Neuronal Network (ANN), and a Bayes classifier.

RF is a non-parametric classifier using an ensemble of Classification and Regression Trees (CARTs) by bootstrapping and replacement [86]. It is a fast algorithm, less sensitive

to the quality of training samples and overfitting, and well suited to handling high data dimensionality and multicollinearity [85], here implemented with a maximum of 2500 trees. As a simpler implementation, a binary DT utilizes a sequential approach by recursively partitioning the input data [87]. Therefore, it is computationally fast without statistical assumptions but also prone to overfitting [87,88]. As non-parametric statistical learning techniques, SVMs also make no assumptions about data distributions [89]. They are "based on the concept of structural risk minimization (SRM), which maximizes and separates the hyper-plane and data points nearest the spectral angle mapper (SAM) of the hyper-plane" [90] (p. 7). They are considered to be well-performing, robust, and efficient classifiers that can handle limited training samples, while the parameter assignment and especially the kernel choice can be difficult [89,90]. The non-parametric KNN algorithm assigns classes by analysing the most common class of a certain number of nearest neighbours k (here: k = 32) [88,91]. KNN is a relatively simple algorithm using instance-based learning. However, the classification process is slow and especially sensitive to the data structure [88]. The feed-forward ANN applied here as multi-layer perceptrons (MLPs) is a non-parametric classifier constructed as a mathematical equivalent to a human nervous system [90]. It was trained by using a sequential back-propagation algorithm to minimize the error between the MLP output and the training data [90]. As a relatively complex algorithm, parameter specifications can be challenging and tend towards overfitting [88]. As the only parametric classifier, a Bayes Classifier for normally distributed data (Normal Bayes Classifier, NBC) was utilised as a probabilistic approach to classification. While efficient and simple to implement, the NBC is based on the Bayes Theorem, which assumes the features to be independent [92].

The classifiers were designed independently, without interactions in a "parallel combination" [50] (p. 4767). In a second step, the outputs of the classifier pool were combined using the Dempster–Shafer framework [49]. Known as the theory of belief functions or evidence theory, the framework is particularly suited to handling uncertain information [49,50]. To fuse the output of the multiple classifier system, for each pixel, the class label containing the maximum of the Belief Function was chosen as the mean of the Dempster–Shafer combination of Masses of Belief [93]. Here, precision was used as measurement for the Masses of Belief based on the confusion matrices from the pool of classifiers.

Finally, a majority filter with a 3×3 kernel size was applied to the classified images to smooth the output while preserving detail by replacing single pixels in homogeneous areas using majority voting based on neighbouring pixels. The resulting classification maps for each year were then used as input for the change detection process compared to the subsequent years, carried out using the Orfeo Toolbox.

2.4. Accuracy Assessment

To evaluate the accuracy of the classification and thus the reliability of the change detection results, accuracy assessments were conducted for every image classification using the Orfeo Toolbox and QGIS (version 3.22.7).

A reference dataset was created for every image based on high resolution Google Earth imagery and corresponding aerial images. A stratified random sampling method was applied to ensure an equal selection chance while preventing an overrepresentation of dominant land cover classes. The reference dataset included 100 validation samples per class and year, in total 1000 samples, which were not used to train the hybrid ensemble model.

A confusion matrix was created for each classified image, and standard performance measures such as overall accuracy, producer accuracy, and user accuracy, as well as the Kappa coefficient were derived [94].

2.5. Intensity Analysis

To quantitatively characterise the complex and long-term LULCC dynamics for the entire study area, an intensity analysis was performed following Aldwaik and Pontius [95]. The mathematical framework allows for unified measurements of size and stationarity of

LULCC dynamics at three analysis levels by examining the degree to which changes are non-uniform [95]. First, the interval level examines the multi-temporal size and speed of LULCC; Second, the category level reveals active and dormant classes by examining the size and intensity of class gains and losses. Third, the transition level examines size and intensity between the different classes [95].

Here, the analysis of the first two levels of intensity analysis was performed using the script developed by [95] (version 2014) in Microsoft Excel. Since the method requires equal time intervals for meaningful results, the first scene from 1974 was excluded from analysis because it constitutes a baseline outside the five-year intervals of the other scenes from 1990 to 2021.

3. Results

The analyses described above resulted in eight novel LULC products for the Ayeyarwady Delta. They described the LULCC dynamics between 1974 and 2021, which are presented in the following section (see Figures 3 and 4). The results of the intensity analysis are displayed in Figure 5 (level 1) and Figure 6 (level 2).

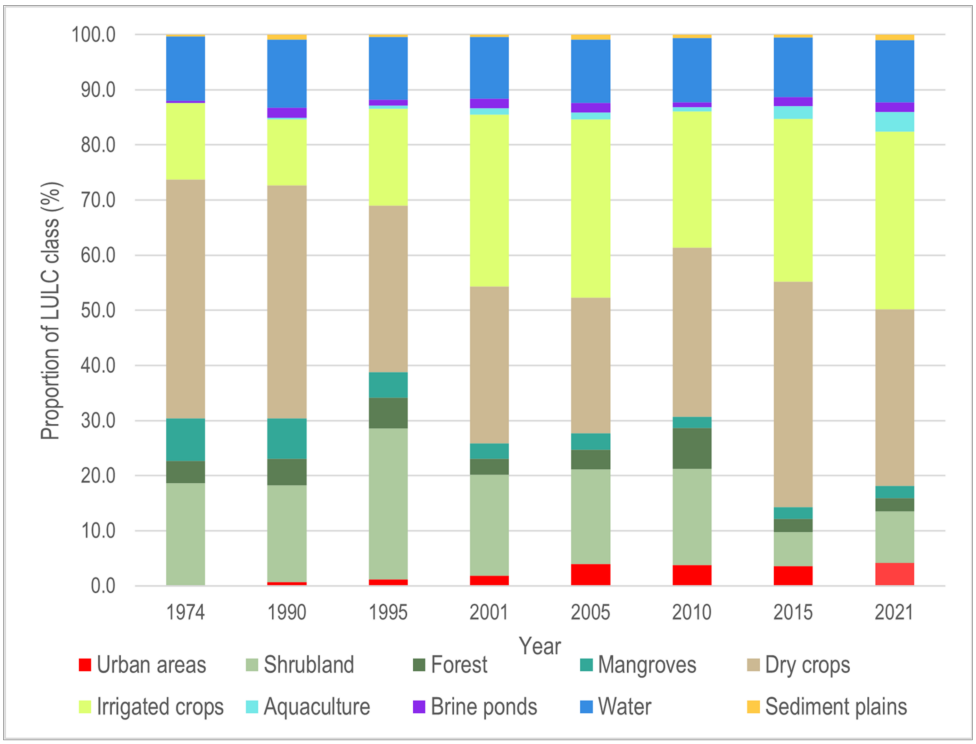

Figure 3. LULC compositions of the Ayeyarwady Delta from 1974 to 2021. Individual share of LULC classes can be obtained from the size of the 100% proportion (individual class height).

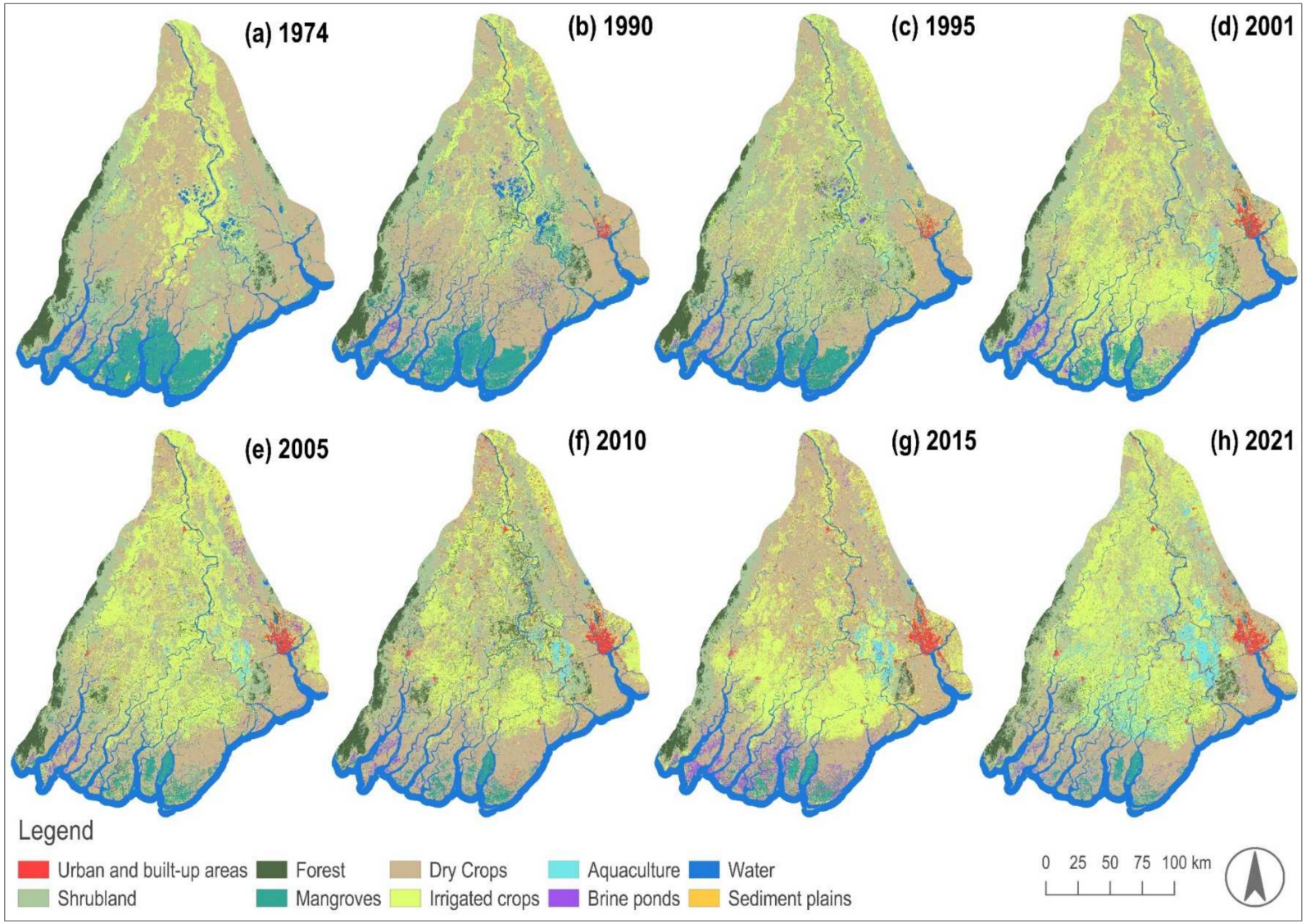

Figure 4. Land cover classification products for the Ayeyarwady Delta from 1974 to 2021 (**a**–**h**).

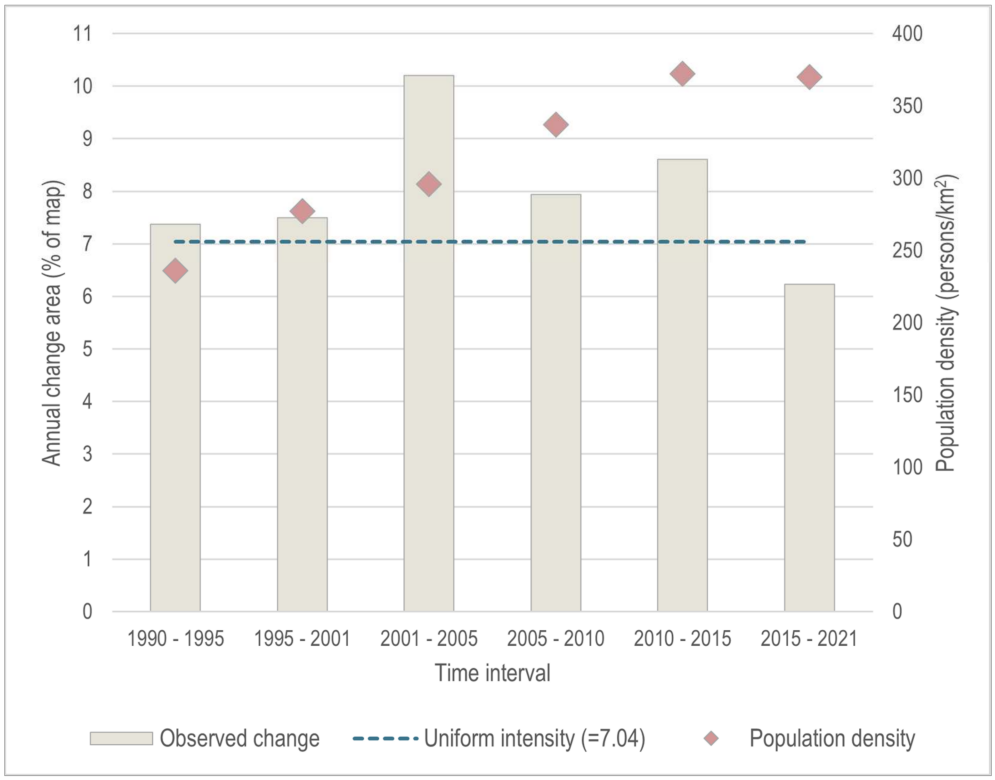

Figure 5. Rate of annual landscape changes in the Ayeyarwady Delta between 1990 and 2021. The uniform intensity line represents the annual rate of change assuming a spatiotemporally equal distribution. Population density as ambient population is taken from corresponding LandScan data for the delta.

3.1. Multiple Classifier System Accuracies

The results of the accuracy assessment (the eight confusion matrices) are shown in Tables S1–S8 (see Supplementary Materials). The overall accuracies were consistently above 90% except for the classification based solely on Landsat 1 data in 1974 (78%). The classification for the most recent year, 2021, yielded the highest overall accuracy of about 95%. The overall kappa coefficients were slightly lower but in the same range of values above 0.9, indicating a strong level of reliability. An exception was, again, 1974 (0.75), although still indicating a moderate level of reliability.

Accuracy for the individual LULC classes was generally high, with user accuracies higher than 0.90 in almost all years, except for the urban and built-up areas, aquaculture, and brine ponds classes. The user accuracies of the urban and built-up class ranged between 0.29 (1974) and 0.98 (2021), with interferences mainly occurring with classified shrubland and irrigated areas. The user accuracies of the aquaculture ranged between 0.05 (1974) and 0.94 (2021), and those of the brine pond classes ranged between 0.68 (1974) and 0.89 (2021). Here, misclassifications occurred mainly between the two classes themselves. The classes with particularly high user accuracies close to 1 included the forest, mangrove, and water classes.

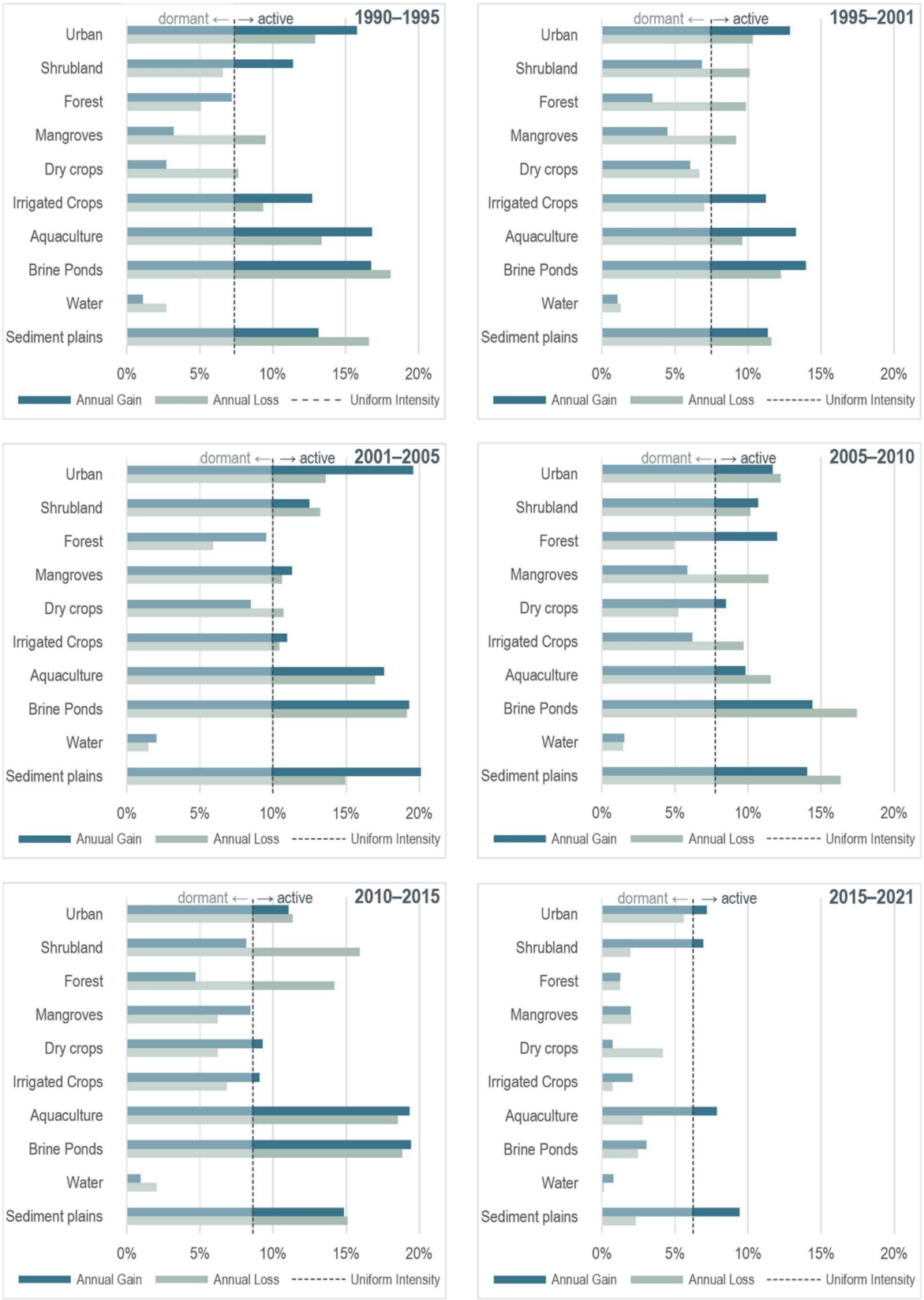

Figure 6. Category intensity analysis for six time intervals between 1990 and 2021 in the Ayeyarwady Delta showing the intensity of annual gains and losses within each LULC class.

3.2. Characterizing Land Use Dynamics

The analysis of the LULCC dynamics in the Ayeyarwady Delta over the last 50 years revealed generally high intensities, as can be seen in Figure 5. On average, one-third (36%) of the entire study area is affected by LULCC in each time interval. This represents a uniform annual change of 7.04%.

The land use dynamics were lowest in the first (1990–1995) and the last (2015–2021) time interval, with a total affected area of about 37% and 15% and an annual change intensity of 7.4% and 6.2, respectively. LULCC dynamics were highest from 1995 to 2001 with 45% (annual change of 7.5%). There was another peak of about 43.1% and an annual change rate of 8.6% between 2010 and 2015. Thus, the LULCC dynamics showed some similarities with the overall population trend in the Ayeyarwady Delta (see Figure 5).

The second part of the intensity analysis on trends of gross losses and gains among the different LULC classes is presented in Figure 6, specifying active or dormant land cover categories with regards to the category-level uniform intensity for each time interval. The most dynamic category, with constant active gains but also active losses throughout all time intervals except the most recent, included the brine ponds and sediment plains classes (Figure 6). This also held true for the urban and built-up classes, which showed dormant losses only in the most recent time interval between 2015 and 2021. Similarly, in the aquaculture class, dormant losses occurred only in the two most recent time intervals, whereas previously it was exclusively actively gaining and losing. The forest class experienced dormant losses as well as gains in general, with the exception of two time intervals in the middle of the study period (1995–2001 and 2010–2015) in which active losses occurred. In the mangroves' class, active losses occurred consistently and only in the most recent two time intervals did the class's losses and gains become dormant. In contrast, the irrigated crop class had predominantly active gains. This was in contrast to developments in the dry crop class, which showed mainly dormant gains over the same period. The shrubland class was the only one to show mixed dynamics over the entire study period.

3.3. Identifying Potential Disaster Risk Drivers Related to LULCC

3.3.1. Urban Growth

The intensity analysis revealed the high dynamics of the urban class, which included dense urban areas and impervious surfaces such as roads, airports, and industrial districts as well as sparsely built-up areas, having a higher proportion of urban green, especially in rural areas. Until 2001, the proportion of the urban and built-up areas' classes in the entire study area was below 2%. Settlement areas were concentrated in the (pre-)colonial historical centres such as Yangon in the east and Pathein in the west of the delta. Urban sprawl dynamics mostly occurred due to the development of the former capital and present megacity of Yangon. Numerous towns existed in the 1970s in different parts of the delta, partly as local trade centres, partly at strategic positions in the immediate vicinity of the river systems, including Bogale and Pyapon in the southeastern lower delta or Hinthada at the delta apex in the north.

By 2005, there had been a significant increase of urban areas, first by about 70% from 1990 to 1995 and from 1995 to 2001 and then by more than 100% between 2001 and 2005. The total share of this class in the study area also more than doubled to just about 4% (1600 km^2). These dynamics were interrupted by a decline of about 5% between 2005 and 2010, which continued in the following period from 2010 to 2015. However, in the most recent study period, from 2015 to 2021, there was again a positive trend (+17%; 230 km^2), with an increase in the share of the total area to just above 4%. These growth rates during the study period are accompanied by increasing urban sprawl dynamics. This expansion is concentrated mainly along the river courses and in agriculturally dominated rural areas, such as Myaungmya in the southeast of Pathein or Kyonpyaw in the upper delta region.

Overall, urban areas increased from less than 100 km^2 at the beginning of the study period to about 1640 km^2 in 2021. This represents an increase of about 5700% and marks one of the strongest LULCC dynamics in the Ayeyarwady Delta. However, it should be

noted that the share of urban areas located below 5 m in the delta has increased by about 300% and those below 10 m by about 400%. Thus, in 2021, about 200 km^2 (<5 m) and 750 km^2 (<10 m) constituted urban areas located in low-lying areas, which can be prone to flooding and the effects of sea level rise.

3.3.2. Agricultural Transition

Agricultural areas are the dominant landscape feature in the Ayeyarwady Delta. They already accounted for 57% of the delta area at the beginning of the study period in 1974. Overall, the class is subject to slight fluctuations but is still relatively stable, covering 50% to 65% (ca. 26,000 km^2) of the study area.

The highest increases took place throughout the first half of the study period, i.e., between 1990 and 2001, with rates of 20% to 70%. This increase was followed by two intervals of stagnation and slight decreases between 2001 and 2010, followed by a sharp increase in the following period (+27%, 6000 km^2). The most recent interval studied was again characterised by a moderate decrease of almost 9% (−2200 km^2). In 2021, agricultural use accounted for 64% of the delta area (about 26,000 km^2). Overall, agricultural land in the delta increased by about 12% between 1974 and 2021, which is equivalent to an increase in land area of about 3000 km^2.

Significant, however, are the major changes of the two agricultural classes studied, namely dry and irrigated crops, which developed contrastingly. The dry crop areas occupy most of the central delta. The expansion of this class is taking place at the expense of forest and other natural vegetation areas in the upper delta and mangrove loss in the lower delta. However, the dry crop area decreased by about 26% during the entire study period. While this class accounted for around 85% of the total agricultural area of the delta at the beginning, the proportion decreased to about 50% in 2021. This trend was interrupted only by two intervals of increases from 2005 to 2010 and 2010 to 2015. However, during the following most recent study interval between 2015 and 2021 a continued overall downward trend with a loss of 22% (−3500 km^2) could be identified.

In contrast, the irrigated agricultural area increased significantly during the study period. While the class made up 25% of the total agricultural area in 1974, it occupied about 50% in 2021, thereby covering about 32% (13,000 km^2) of the total study area. Initially, irrigated areas were only present in linear stripes along and in between river banks, not much further south than the town of Wakema about 450 km from the coastline. While these areas also expanded until 2021, most area gains were obtained by the formation of a large contiguous arc-shaped area dominated by irrigated agriculture, which extended southwards from Pathein to Yangon. This increase started between 1990 and 1995 with 46% (2203 km^2; 41 km^2/year) and was most severe between 1995 and 2001 with an increase of about 78% (5412 km^2, 1353 km^2/year), reduced to a moderate increase of about 4% from 2001 to 2005. The period between 2005 and 2010 is the only interval since 1974 where irrigated agricultural areas were decreasing by about 24%. In the two latest time intervals, the upward trend continued with an increase of about 20% and 9%, respectively. Overall, the irrigated crop class increased by about 130% between 1974 and 2021 and gained an area of about 7000 km^2. Those dynamics are among the most significant LULCC in the Ayeyarwady Delta.

3.3.3. Deforestation

Both woodland classes in this study, closed broadleaf forest and mangroves, suffered from deforestation. In 1974, the forest class covered less than 5% of the delta area, concentrated almost exclusively on the foothills of the Rakhine mountain range in the western part of the delta. Phases with significant forest losses were 1995–2001 (−48%; −1073 km^2) and 2010–2015 (−67%; −2000 km^2), alternating with phases of gross forest gains of about 17% in the first two study intervals, most significantly from 2005 to 2010 (+110%; 1543 km^2) and an almost stable phase from 2015 to 2021 (+0.3%), as can be seen in Figure 6. Thus, the development of the forest stands during the study period followed a specific pattern in that

one period of loss occurred after two intervals of regeneration. The maximal expansion of forest areas was reached in 2010 with about 3000 km^2 (ca. 7%) of the total delta area. Nevertheless, the forest coverage in the delta decreased about 40% between 1974 and 2021, with a remaining forest area of about 1000 km^2 in 2021, 3% of the total delta.

In 1974, mangroves covered about 8% (3000 km^2) of the entire delta, mainly located on the southern river mouths under coastal saline influence, forming a fringe along the river courses near to the coast. The highest mangrove losses occurred between 1990 and 2001, with an area decrease of about 38% per five-year interval. This decrease corresponded to annual deforestation rates ranging from 8.4 km^2 (1974–1990) to 219 km^2 (1990–1995) and 118 km^2 (1995–2001). These losses were mainly due to expanding aquaculture, brine pond, and agricultural areas. This period was followed by a short increase phase between 2001 and 2005, with a mangrove area gain of 5% (14 km^2/year). Another 366 km^2 of mangroves (31%) were lost in the following period between 2005 and 2010 (73 km^2/year). The most recent periods showed slight area gains of about 35 km^2 from 2010 to 2015 (+4%) and an almost stable period (-0.2%, -2 km^2) between 2015 and 2021. In 2021, mangroves covered about 2% (850 km^2) of the entire Ayeyarwady Delta. The remaining stands have retreated significantly towards the coast and are highly fragmented. If at all, only a few residual stands can be found along the river courses. Only the Meinmahla Kyun Wildlife Sanctuary remains excluded from these dynamics. A patch size analysis revealed that connected areas decreased from a maximal size of 606 km^2 (mean = 0.05 km^2 $\pm$ 3.02) in 1990 to 103 km^2 (mean = 0.02 km^2 $\pm$ 0.58) in 2021. Overall, the mangrove areas decreased by 72% between 1974 and 2021, corresponding to an area loss of 2200 km^2. The mangrove class experienced the most severe decrease among all analysed LULC classes.

3.3.4. Expansion of Cultivated Aquatic Surfaces

Cultivated aquatic surfaces, here represented by the aquaculture and brine pond classes, were hardly present in 1974 at the beginning of the study period, covering less than 1% of the delta (154 km^2). Together, cultivated aquatic surfaces are among the LULC classes in the Ayeyarwady Delta with the highest rates of spatial increase between 1974 and 2021 (+1300%; 2000 km^2).

The expansion of brine ponds started earlier than that of aquacultural areas with an increase of 364% between 1974 and 1990 (560 km^2; 35 km^2/year) but remains far behind in terms of spatial extension (see Figure 3). Both classes increased sharply, particularly between 1995 and 2001: aquaculture by 108% (233 km^2; 39 km^2/year), and brine ponds by 64% (270 km^2; 35 km^2/year). Between 2001 and 2005, this development was reduced to an increase of 8% and 3%, respectively. Both classes suffered significant losses between 2005 and 2010 with Nargis hitting in 2008, the coastal brine ponds class (-51%; -367 km^2) more severely affected than the aquaculture class (-30%; -145 km^2) located inlands. Both classes recovered in the following period from 2010 to 2015 and recorded their highest growth rates since 1974/1990 with 162% (550 km^2; 110 km^2/year) for aquaculture areas and 90% (300 km^2; 63 km^2/year) for brine ponds. This growth continued for both classes in the following period. Aquaculture areas increased again by nearly 60% (520 km^2; 87 km^2/year) between 2015 and 2021, now covering about 4% (1400 km^2) of the entire delta area. Brine ponds increased to a much lesser extent of 4% (30 km^2), covering 2% (700 km^2) of the delta in 2021.

Overall, aquacultural use increased between 1974 and 2021 by 1400 km^2. This development originated from an aquaculture cluster in the townships of Maubin and Twantay in the west of Yangon. Especially since 2010, individual, smaller clusters also formed in central and northeastern areas of the upper delta. This expansion has been taking place largely at the expense of natural wetlands and associated vegetation communities (see Figure 4). Still significant but less extensive was the increase of brine ponds between 1974 and 2021 by 540 km^2. The distribution is almost exclusively limited to the two near-coastal towns and townships of Labutta and Pyapon in the south of the delta, covering the estuaries. Hence, the brine pond class mainly replaced the mangrove areas and contributed

significantly to their fragmentation. Cultivated aquatic surfaces are among the most intense LULCC dynamics in the Ayeyarwady Delta, while at the same time they are spatially highly concentrated.

4. Discussion

4.1. Land-Use Related Potential Disaster Risk Drivers in the Ayeyarwady Delta

The eight novel LULCC products presented and analysed in this study describe long-term land use dynamics in the Ayeyarwady Delta thematically detailed for almost five decades between 1974 and 2021. As to be expected in a highly dynamically deltaic environment, the analysis shows generally high LULCC intensities throughout the study period. The first identified phase of this intensification from 1990 onwards coincided with the end of the so-called Burmese Way to Socialism and the following transition towards a market-oriented economy after 1988. Dynamics increased again in a second phase starting in 2010 in which the delta transformed with the highest change rates. That phase started—as could be proven—after 2010 with the beginning of the economic and political opening policies, with a peak between 2015 and 2021, when—induced by internationalization and globalization dynamics—the influx of national and international capital and development activities rose, and infrastructural upgrading gained a high pace, thus exacerbating urban and settlement expansion in the delta. After 2008, the effects of Cyclone Nargis could be identified between 2005 and 2010, causing a major disruptive disturbance for almost all classes, which partly lasted into the following interval, thereby indicating the long-term consequences of such events.

In a next step, among these identified LULCC dynamics, a more detailed analysis was performed on those that could act as potential disaster risk drivers based on the UNDRR global assessment. For the Ayeyarwady Delta, these include urban growth, agricultural intensification, deforestation, and mangrove loss and the expansion of cultivated aquatic surfaces. While all of these LULCC dynamics generally have the potential to increase risks, not all seem to be equally influential in the Ayeyarwady Delta.

Urban areas expanded in the Ayeyarwady Delta rapidly from 2001 onwards. Although still moderate compared to other mega-urban deltas, the low-lying urban areas, which are particularly threatened by flooding and sea level rise, have increased by about 300% (<5 m) and 400% (<10 m). The potential threat of such a development becomes evident in a detailed analysis showing the abrupt decline of settlement areas after Cyclone Nargis hit the delta in 2008, causing more than 138,000 fatalities [96]. The Post-Nargis Joint Assessment found that more than 80% of rural houses were made of easily constructed wattle-and-daub walls, considered to be the primary cause of widespread destruction [14]. Furthermore, as the expansion of urban areas is usually associated with water channel regulation, increasing imperviousness and declining ecosystem services [97], such developments can potentially lead to growing risk exposure. Urban growth is contributing to intensifying sediment mining activities in the Ayeyarwady Basin, especially for coarse sand and gravel as valuable construction materials [46,98]. These activities can create and enhance bank and coastal erosion and can contribute to altering riverbed geomorphology and increasing flood risk [46]. Furthermore, land subsidence adds to increasing flood risk, especially when the sediment balance can no longer be maintained [28,99]. For Yangon, the largest city in the east of the delta, land subsidence analysis conducted by van der Horst et al. [100] found velocity differences over 22 mm/year, locally exceeding 110 mm/year, mainly attributed to groundwater extraction for domestic supply and secondarily to additional building loads on the surface [100]. While dynamics of this dimension are not expected for the entire delta, where urban area coverage is still below 5%, the results of this study show a trend towards settlements located in hazard-prone areas. Therefore, the current patterns of urban expansion in areas below 5 m and 10 m is a disaster risk driver in the respective areas.

Agriculture is the dominant landscape feature in the Ayeyarwady Delta, covering already 57% of the area at the beginning of the study period in 1974. The transformation of a predominantly natural to an agricultural landscape goes back to the 19th century, described

by the British historian Adas [33] (p. xiii) as "one of the most remarkable episodes in the modern history of colonialisation", where the British transformed the delta from a densely forested and sparsely populated area into one of the largest areas for rice export. This study identified a second major transition within the agricultural system of the delta, namely, the shift from dry crops towards the now dominant irrigation system. While irrigated areas accounted for only 24% of the total agricultural area in 1974, they rose substantially to 50% in 2021, increasing by about 130% in almost 50 years. However, precise assessments of the type of irrigation cannot be made at the resolution used by this study and should be the subject of further research. This development is accompanied by the decrease of non-irrigated areas by 26%, declining from a share of 76% of the total agricultural area in 1974 to 50% in 2021. These dynamics were only temporarily interrupted by the effects of Cyclone Nargis. These results are in accordance with Sakai et al. [101], who found an increasing annual cropping intensity from 1.1 ± 0.4 in the 1980s to 1.4 ± 0.5 in the 2010s, marking a shift from a single to double cropping system in the delta to a much larger extent.

The necessary resources of capital, technology, and know-how were realized by national efforts with the help of international actors and made possible by a series of national legislation following the introduction of a market-oriented economy after 1988. Among those laws were the Foreign Investment Law (1988), the State Economic Enterprise Law (1989), and the Wasteland Instruction (1991), permitting certain private sector, international activities and large-scale land concessions. Two World Bank projects in the 1970s as well as the "Lower Burma Paddyland Development Project" and the "Irrigation Project I Burma" initialized the development of cultivable land and the reclaiming of abandoned paddyland as well as the widespread construction of mainly pump irrigation infrastructure accompanied by minor flood embankments [102,103]. Of particular importance was the nationwide Summer Paddy Program, implemented in 1992, introducing new rice varieties, cropping practices and irrigation facilities and making rice cultivation in the dry season compulsory [101,104]. These measures correspond to the sudden increase of irrigated areas since 1990 and especially 1995, as identified in this study.

The main limiting factor of this development in the Ayeyarwady Delta is saline intrusion [43]. As the irrigation infrastructure in the delta is regarded to be underdeveloped, using mainly surface and especially river water, increasing salinity of the water is accumulated in the soil and reducing the arable land [43,105]. This development will most likely be exacerbated due to sea-level rise and climate change [43,106]. In the context of the medium (RCP4.5) and high (RCP8.5) IPCC AR5 emission climate change scenarios, the average yield increase of early rice (harvest in May) is expected to increase about 10%, but the reduction of late rice (harvest in October) can be up to 50% due to increasing temperatures and variation in rainfall patterns [107]. A household survey of rice farmers in the Ayeyarwady Delta [106] found an overall low adaptive capacity, limited technical and institutional support and networks, as well as insufficient input resources such as seeds and fertilizers. Recent increases of especially irrigated areas in an internationalizing framework, at least as of 2021, may hint at shifting power, land, and capital control from local elites towards national actors and investors mainly from China, India, Malaysia, Thailand, and Vietnam [36,108]. While the identified transition to irrigation within the agricultural system is among the most remarkable LULCC dynamics in the Ayeyarwady Delta, agricultural expansion and intensification seems to be themselves at risk rather than becoming active disaster risk drivers (at least for the studied period, ignoring the initial part of restructuring the natural delta system in British times). In the mid- and long term, the mentioned transition may be leading to serious challenges to maintaining food security as climate change, sea-level-rise, the probability of increasing extreme weather events and resource degradation are likely to rise [105,109].

The main deforestation phases in the Ayeyarwady Delta happened before the start of the investigation period when the British systematically expanded the rice cultivation frontier [33], leaving fragmented residual areas behind. The shift from a forest-oriented to an agricultural-oriented land use between 1997 and 2004, identified for the near-coast located

Tanintharyi Region in Myanmar by Alban et al. [48], was completed in the Ayeyarwady Delta long before the beginning of the investigation period in 1974. The remaining forest cover of 3% of the entire delta has remained relatively stable. However, regular gains and losses between the forest and shrubland classes indicate high transitional dynamics through degradation, fallow land, recultivation, and regeneration, indicating high utilization pressure. In contrast, the mangrove areas almost disappeared between 1974 and 2021, covering only 2% of the delta area in 2021 after a loss of more than 72% since 1974. None of them has a patch size greater than 103 km^2, a reduction of 83% compared to 1990. This trend is confirmed by the results of Webb et al. [36], who found a maximal mangrove patch of 300 km^2 for the year 2011. This corresponds to the overall trend already noted by Heymann and Löffler 1997 [34], with a loss of mangroves by almost 50% by the late 1990s, i.e., the beginning of the investigation presented here.

Again, in overall agreement with the findings of Webb et al. [36] and Yang et al. [110], this analysis shows, first, that conversion to agricultural land was responsible for most of the mangrove loss in the past 50 years, and, second, that the rapidly expanding aquaculture and salt farming areas have been considerably co-responsible for deforestation in the delta. While this change is accompanied by extraction for fuelwood, charcoal, and non-timber forest products [65,111], the increase in deforestation since the introduction of the market-oriented economy and advancing privatization may suggest that deforestation in the Ayeyarwady Delta is increasingly driven by national efforts to intensify food production and the internationalization of agro-business. Among one of the few mangrove areas remaining intact in the delta is the Meinmahla Kyun Wildlife Sanctuary, where no significant deforestation dynamics can be found (see also [36]). Since this area became an ASEAN Heritage Park and, since 2017, has been under the protection of the global Ramsar Convention on Wetlands, the integrity of this sanctuary indicates the effectiveness of those protection measures and their possible transferability to other areas.

While Webb et al. [36] forecast the complete deforestation of mangroves in the Ayeyarwady Delta by 2035 based on business-as-usual scenarios, results presented here are indicating a recent stabilization with slight increases between 2010 and 2015 (+7 km^2/year) and an almost stable period from 2015 to 2021 (−0.2%). Future investigations may show whether this is solely due to the fact that all relevant areas have already been cleared and a mere temporary stabilization is taking place or whether national protective efforts, including community-based restoration projects, have become effective. Moreover, the recorded loss and fragmentation of mangrove areas is associated with a decline in biodiversity and ecosystem services. In particular, their ability to protect the shoreline as bioshields, thereby mitigating high energy events such as tropical cyclones by breaking the force of waves, trapping sediment, and preventing coastal erosion [31,45,46,61,112], effectively no longer exists and has already been associated with the danger of increasing the damage of torrential winds and extensive flooding in the Ayeyarwady Delta [33,113]. Thus, the significant loss of mangrove areas and their protective function are some of the active disaster risk drivers, especially in the low-lying areas of the lower Ayeyarwady Delta.

Finally, the identified changes address the expansion of cultivated aquatic areas in the delta. This class only became evident during the study period, as aquaculture was first introduced in the mid-1960s [114]. Aquaculture areas as well as brine ponds covered less than 1% of the study area in 1974 but were, respectively, increasing towards 4% and 2% until 2021. Especially the expansion of aquaculture was driven by the Aquaculture Law (1989), facilitating the conversion of so-called wasteland to fish ponds [115]. This conversion initially took place on natural and semi-natural wetlands and later at the expense of agricultural areas. This finding is consistent with observations by Belton et al., who found that "flood control schemes constructed in rice growing areas of the Delta in the late 1990s to intensify rice production made the land more suitable for pond farming" [115] (p. vi). The state-facilitated rice agriculture created a sector dominated by large companies from the start, as small-scale farmers were not allowed to convert paddy fields to fish ponds [115]. Nevertheless, higher income and employment generation increasingly attract

small and medium enterprises in both on- and off-farm segments, leading to an aquaculture sector with a dualistic structure [115]. In addition to the observed spatial extension during the study period (+2666 km^2), there is a significant yield intensification of fish per acre [115].

Spatial expansion as well as intensification can have significant impacts on the delta system, adjacent ecosystems, and human health due to toxic waste pollution such as antibiotic impacts, dissolved oxygen, and nitrate [112]. For the last two values, thresholds have already been exceeded in samples from the delta [65]. Furthermore, high levels of groundwater extraction required for aquaculture can induce land subsidence up to 1 m every 4 years, as shown, e.g., by Higgins et al. [116] for aquaculture facilities in the Yellow River Delta and by Hung et al. [117] for the coastal Chiayi area in Taiwan. However, since these dimensions of aquaculture expansion have not been reached in the Ayeyarwady Delta so far, those dynamics may act in a different order of magnitude. Nevertheless, the spatial development dynamics of the agricultural sector during the last 50 years point to a potential disaster risk driver in the future. In contrast, brine ponds have played a major role in deforestation of the coastal mangrove stocks and would currently impede potential reforestation efforts. Therefore, despite their small proportion in terms of area, they are already, to a certain extent, a disaster risk driver that may increase.

4.2. Hybrid Ensemble Classification for Long-Term and Multi-Temporal LULCC Analyses

The generated LULC map products provide long-term, multi-temporal, and area-wide information about LULCC dynamics in the Ayeyarwady Delta on a consistent and thematically detailed level not present in previous studies. The classification method applied in this study resulted in high overall accuracies above 90%, comparable to and slightly higher than similar studies in other deltaic regions (e.g., [76,118,119]). These accuracies confirm that ensemble learning models for classification are capable of outperforming single classifiers, even in highly complex and heterogeneous environments. Another main advantage of this approach is the use of freely available remote sensing data and open-source software, foregoing ancillary data and so-called expert rules prone to subjective influences.

Although training dataset composition is crucial for the classification's accuracy, and field surveys are still the preferred choice for obtaining valid ground truth data [73], the results of this study support the increasing practice of using high-resolution imagery from Google Earth and aerial photographs as substituting, effective, and time- and cost-efficient alternatives for a detailed LULCC analysis. Therefore, the applied method is a possibility for gaining objective long-term information in areas with poor data and poor accessibility.

The main challenge of this remote sensing approach was the long-term availability of satellite data with respect to the frequent cloud coverage in the region, limiting the analysis to the dry season. While this allows for identifying irrigated areas, the spectral separability of agricultural areas such as fallow land, sowing, and early state vegetation from other classes remains difficult. The integration of multi-seasonal data can improve this differentiation, while intra-annual time series, such as those conducted by Torbick et al. [42] for rice agriculture in Myanmar, would offer deeper insights into the agricultural system of the delta such as detailed crop types, harvest cycles, and other phenological characteristics.

The nearly five-year interval time series spanning almost half a century created and analysed in this study began shortly after the initiation of the Landsat mission in 1972, the only archive in the world providing global data for such a long period of time. However, the use of this data also limits the spatial resolution of the analysis to 30 m, and 60 m for the earliest time period (1973/1974) covered by Landsat-1 MSS. This low resolution is particularly problematic in a study area such as the Ayeyarwady Delta, which is characterised by extremely heterogeneous and highly fragmented land cover. For example, Kuenzer et al. [24] point out that mangroves often occur as strips smaller than 50 m in fringe coastal zones. Dispersed settlements with a high share of vegetation and separated farmsteads scattered throughout the rural areas of the delta are also difficult to identify, leading to interferences with mosaic vegetation. On the one hand, the medium spatial resolution leads to a loss of detail and selectivity, while on the other hand, a higher resolution would

lead to a higher degree of spectral variations, complicating the analysis in large-scale areas. This issue was partially addressed by pan-sharpening to a 15 m resolution of Landsat-7 and Landsat-8 data for the three periods of 2001, 2015, and 2021. Unsurprisingly, the overall accuracies for those years were higher (91% to 94%), also caused by the overall better sensor equipment. In contrast, the 1973/74 accuracy using 60 m × 60 m Landsat-1 MSS imagery was the lowest (78%) and therefore used as baseline information but not always included in the direct comparison of the time series. Additionally, the classification was improved for the two most recent time periods, 2015 and 2021, through the integration of Sentinel-1 data.

Thus, this study confirms the great benefit of the synergistic use of optical and radar data, not only because of the all-weather capability but also for the specific microwave backscattering characteristics of water-loaded classes, such as rice paddies, aquaculture, and inundated areas [24,42,120,121]. The classification accuracy was most improved by using different spectral indices, which significantly increased the separability of the individual LULC classes. The location between land and sea, with intertidal effects and a high water content of many LULC classes, poses a major challenge for classifying delta landscapes in regard to spectral mixture. The NDTI is used as an indicator of water quality (e.g., [122]), but Sakai et al. [43] demonstrate a linear relationship between turbidity and electrical conductivity and thus also a relationship with river water salinity. In this study, the NDTI helped to separate the actual water, which includes not only sea and river water but also numerous standing waters and reservoirs, including the aquaculture and the brine pond classes. The mapping of mangroves has been termed "one of the most demanding tasks in remote sensing" [112] (p. 913) due to the high degree of components influencing the signal, such as plant and leaf geometry, underlying mudflats, soils, and water surfaces [112]. When hyperspectral imagery is not available, this task often requires a high degree of interactivity [112]. This study shows that the CMRI index developed by Gupta et al. [81] and the easily objectifiable topographic mask proposed by Yancho et al. [82] can be combined with little interactivity to identify mangroves with great accuracy, even in medium-resolution indices. The successful application of both measures underlines the advantages to be expected from using them for medium-resolution studies in coastal areas.

Despite the relatively high accuracy values in relation to the spatial resolution, the per-pixel classification method used reinforces the spectral mixture issue in mid-resolution image data. Above all, this issue applies to the various stages of salt farming and their differentiation from aquaculture, urban areas with a high share of vegetation, and the intermediate stages of irrigated agriculture and different types of semi-natural wetlands. In this context, objected-based methods could increase classification accuracy, as they additionally consider the relative location and the shape of surfaces. This improvement has already proven to be advantageous for the distinctive rectangular shape of aquaculture ponds (e.g., [123]) and could also facilitate the identification of building blocks and agricultural patches. However, object-based methods are still mainly applied when investigating areas less than 300 ha using high-resolution data [124], which significantly limits the effective use in the study area of the Ayeyarwady Delta, covering about 40,000 km^2. Another improvement option may be the use of sequential classification techniques to increase the spectral separation of LULC classes in highly complex environments, as proposed, for example, by Ottinger et al. [76].

As the findings of this study offer valuable insights on long-term LULCC dynamics for the entire Ayeyarwady Delta, the potential of intra-annual time series and multi-source data for more detailed information on smaller scales could be a focus for further research.

5. Conclusions

This study presented a novel, area-wide, long-term, and multi-temporal analysis of land use dynamics in the Ayeyarwady Delta in Myanmar spanning nearly five decades from 1974 to 2021 in five-year intervals, addressing a general lack of precise and consistent data in one of the least studied mega-deltas in the world.

A hybrid ensemble model consisting of six different machine learning classifiers using 50 Landsat and Sentinel-1A images and various spectral indices was developed for the Ayeyarwady Delta. Due to the data-poor conditions, but also to ensure the greatest possible objectivity, ancillary data and classification rules based on expert knowledge were not considered. The approach was conducted using only freely available data and open-source software. The achieved accuracies of more than 90% are promising, despite limited availability of cloud-free data and some uncertainties due to spectral mixture issues, most notably in the urban and built-up areas, aquaculture, and brine ponds classes.

The analysis revealed high LULCC intensities throughout the study period, most notably during the first two periods (1974–1990, 1990–1995) immediately after the introduction of a market-oriented economy after 1988 and the most recent periods (2010–2015 and 2015–2020) under the increasing influence of national development activities, internationalization, and globalization dynamics. The major identified potential risk-relevant LULCC dynamics include urban growth towards low-lying areas, expansion of irrigated agricultural areas, mangrove deforestation, and the expansion of cultivated aquatic surfaces. Urban growth, mangrove loss, and the associated expansion of brine ponds represent active disaster risk drivers in the respective parts of the Ayeyarwady Delta, with high intensity in the corresponding LULC classes. The expansion of aquaculture may become a potential future disaster risk driver if recent growth rates are maintained. In contrast, the agricultural areas seem to have reached their maximum extent and are now themselves at potential risk, particularly where irrigation systems are a necessity.

The results of this study support a number of recommendations to avoid increasing or creating potential disaster risk: (1) Urban areas below 5 m have increased about 300% and those below 10 m about 400%, new settlement areas only outside of particularly hazard-prone areas may need to be considered, and remote sensing and impact simulations could aid appropriate planning processes. (2) Maintaining food security in the future through irrigation-dependent agriculture is likely to present growing challenges from, e.g., climate change, salinization, and land degradation effects; and measures aimed at strengthening adaptive capacities, diversification of crops, and farming practices and alternative sources to maintain food security may need to be implemented and extended sooner rather than later. (3) Aquaculture—which without doubt could be an important source for income and nutrition—can simultaneously contribute to long-term potential disaster risk creation, since its expansion has not progressed as far as in other deltas; there is still an opportunity to monitor this development closely and to intervene through legislation when necessary. (4) Mangroves and their protective function are almost lost in the delta; recent increases and the effectiveness of protection measures in the Meinmahla Kyun Wildlife Sanctuary offer the opportunity to create awareness, especially based on lingering impressions of the damage caused by Cyclone Nargis, and to restore the delta's natural bio-shield, for instance through replantation or community-based recovery projects, the designation of protected areas, and the enclosure of designated brine pond zones.

The yet unexplored potential for further remote sensing-based studies in the Ayeyarwady Delta lies in using high and very high-resolution data for smaller areas (particularly at a local scale), object-based classification approaches, and intra-annual time series to capture seasonal dynamics in the context of the importance of agricultural developments in the delta. Additional research of specific forms of vulnerability and its shaping through different economic, political and cultural processes, actors, and networks is deemed promising with respect to deepening the understanding of (potential) disaster risk in the Ayeyarwady Delta and to sensitizing for potential risk creation in areas, such as deltas, where negative consequences of developments and agency are often located far away from each other.

Developed with freely available data and open-source software, the thematically detailed and long-term LULCC data created by this study provide a sound basis to support informed decision making towards a more risk-sensitive development in the future (e.g., via consideration in disaster risk management plans and impact models). Remote sensing has proven to be highly suitable for analysing LULCC dynamics in data-poor and complex

deltas such as the Ayeyarwady Delta and can consequently be used in the context of disaster risk monitoring.

Supplementary Materials: The following supporting information can be downloaded at: https://www.mdpi.com/article/10.3390/rs14153568/s1, Table S1: Confusion Matrix for the year 1974; Table S2: Confusion Matrix for the year 1990; Table S3: Confusion Matrix for the year 1995; Table S4: Confusion Matrix for the year 2001; Table S5: Confusion Matrix for the year 2005; Table S6: Confusion Matrix for the year 2010; Table S7: Confusion Matrix for the year 2015; Table S8: Confusion Matrix for the year 2021.

Author Contributions: Conceptualization, A.V.; software, A.V.; validation, A.V.; formal analysis, A.V.; investigation, A.V.; resources, A.V.; data curation, A.V.; writing—original draft preparation, A.V.; writing—review and editing, A.V., F.K., K.S., D.B., H.B., K.K.S., N.W.O., N.A. and Z.N.M.; visualization, A.V.; supervision, F.K., D.B. and H.B; project administration, F.K., D.B. and H.B.; funding acquisition, F.K., D.B. and H.B. All authors have read and agreed to the published version of the manuscript.

Funding: This research incl. APC was funded by the German Research Foundation (DFG), grant numbers KR 1764/28-1, BR 877/37-1, and BR 5023/4-1.

Data Availability Statement: The data presented in this study are available upon request from the corresponding author. The data are not publicly available due to other related not-yet-published publications in the research project. When the research project is fully completed, the data obtained will be made publicly available in an online database.

Acknowledgments: We thank the German Research Foundation (DFG) for the funding of two complementing, international, and interdisciplinary research projects (GZ: KR 1764/28-1, BR 877/37-1, and BR 5023/4-1). We are, furthermore, thankful for valuable reviewer comments on an earlier version of the manuscript.

Conflicts of Interest: The authors declare no conflict of interest. The funders had no role in the design of the study; in the collection, analyses, or interpretation of data; in the writing of the manuscript; or in the decision to publish the results.

References

1. Foley, J.A.; Fries, R.; Asner, G.P.; Barford, C.; Bonan, G.; Carpenter, S.R.; Chapin, F.S.; Coe, M.T.; Daily, G.C.; Gibbs, H.K. Global Consequences of Land Use. *Science* **2005**, *309*, 570–574. [CrossRef]
2. Lambin, E.F.; Turner, B.L.; Geist, H.J.; Agbola, S.B.; Angelsen, A.; Bruce, J.W.; Coomes, O.T.; Dirzo, R.; Fischer, G.; Folke, C. The Causes of Land-Use and Land-Cover Change: Moving beyond the Myths. *Glob. Environ. Chang.* **2001**, *11*, 261–269. [CrossRef]
3. Crutzen, P.J. Geology of Mankind. *Nature* **2002**, *415*, 23. [CrossRef]
4. Winkler, K.; Fuchs, R.; Rounsevell, M.; Herold, M. Global Land Use Changes Are Four Times Greater than Previously Estimated. *Nat. Commun.* **2021**, *12*, 2501. [CrossRef]
5. O'Keefe, P.; Westgate, K.; Wisner, B. Taking the Naturalness out of Natural Disasters. *Nature* **1976**, *260*, 566–567. [CrossRef]
6. UNISDR. *Natural Disasters and Sustainable Development: Understanding the Links Between Development, Environment and Natural Disasters*; Background Paper No. 5; United Nations International Strategy for Disaster Reduction: New York, NY, USA, 2002; p. 10.
7. Lewis, J. The Good, The Bad and The Ugly: Disaster Risk Reduction (DRR) Versus Disaster Risk Creation (DRC). *PLoS Curr.* **2012**, *4*, e4f8d4eaec6af8. [CrossRef] [PubMed]
8. Kelman, I. Lost for Words Amongst Disaster Risk Science Vocabulary? *Int. J. Disaster Risk Sci.* **2018**, *9*, 281–291. [CrossRef]
9. Chmutina, K.; Meding, J. A Dilemma of Language: "Natural Disasters" in Academic Literature. *Int. J. Disaster Risk Sci.* **2019**, *10*, 283–292. [CrossRef]
10. Raju, E.; Boyd, E.; Otto, F. Stop Blaming the Climate for Disasters. *Commun. Earth Env.* **2022**, *3*, 1. [CrossRef]
11. Black, R.; Busby, J.; Dabelko, G.D.; Coning, C.; Maalim, H.; McAllister, C.; Ndiloseh, M.; Smith, D.; Alvarado Cóbar, J.F.; Barnhoorn, A. *Environment of Peace: Security in a New Era of Risk*; Stockholm International Peace Research Institute: Stockholm, Sweden, 2022.
12. Lavell, A.; Maskrey, A. The Future of Disaster Risk Management. *Environ. Hazards* **2014**, *13*, 267–280. [CrossRef]
13. United Nations Office for Disaster Risk Reduction (UNDRR). Underlying Disaster Risk Drivers. Available online: https://www.undrr.org/terminology/underlying-disaster-risk-drivers (accessed on 11 June 2022).
14. United Nations International Strategy for Disaster Reduction (UNISDR). *Global Assessment Report on Disaster Risk Reduction 2009: Risk and Poverty in a Changing Climate: Invest. Today for a Safer Tomorrow*; United Nations: Geneva, Switzerland, 2009.
15. United Nations International Strategy for Disaster Reduction (UNISDR). *Sendai Framework for Disaster Risk Reduction 2015–2030*; United Nations: Geneva, Switzerland, 2015; p. 37.

16. Su, Q.; Chen, K.; Liao, L. The Impact of Land Use Change on Disaster Risk from the Perspective of Efficiency. *Sustainability* **2021**, *13*, 3151. [CrossRef]
17. Nicholls, J.R.; Adger, N.W.; Hutton, W.C.; Hanson, E.S. (Eds.) *Deltas in the Anthropocene*; Springer International Publishing: Cham, Germany, 2020; ISBN 978-3-030-23516-1.
18. Edmonds, D.A.; Caldwell, R.L.; Brondizio, E.S.; Siani, S.M.O. Coastal Flooding Will Disproportionately Impact People on River Deltas. *Nat. Commun.* **2020**, *11*, 4741. [CrossRef] [PubMed]
19. Tessler, Z.D.; Vörösmarty, C.J.; Grossberg, M.; Gladkova, I.; Aizenman, H. A Global Empirical Typology of Anthropogenic Drivers of Environmental Change in Deltas. *Sustain. Sci.* **2016**, *11*, 525–537. [CrossRef]
20. Giosan, L.; Syvitski, J.; Constantinescu, S.; Day, J. Climate Change: Protect the World's Deltas. *Nature* **2014**, *516*, 31–33. [CrossRef]
21. Nienhuis, J.H.; Ashton, A.D.; Edmonds, D.A.; Hoitink, A.J.F.; Kettner, A.J.; Rowland, J.C.; Törnqvist, T.E. Global-Scale Human Impact on Delta Morphology Has Led to Net Land Area Gain. *Nature* **2020**, *577*, 514–518. [CrossRef] [PubMed]
22. Neumann, B.; Vafeidis, A.T.; Zimmermann, J.; Nicholls, R.J. Future Coastal Population Growth and Exposure to Sea-Level Rise and Coastal Flooding—A Global Assessment. *PLoS ONE* **2015**, *10*, e0118571. [CrossRef] [PubMed]
23. Garschagen, M.; Revilla Diez, J.; Dang, K.N.; Kraas, F. Mekong Delta: Between the Prospects for Progress and the Realms of Reality. In *The Mekong Delta System*; Renaud, F.G., Kuenzer, C., Eds.; Springer Environmental Science and Engineering; Springer: Dordrecht, The Netherlands, 2012; pp. 83–132; ISBN 978-94-007-3961-1.
24. Kuenzer, C.; Heimhuber, V.; Huth, J.; Dech, S. Remote Sensing for the Quantification of Land Surface Dynamics in Large River Delta Regions—A Review. *Remote Sens.* **2019**, *11*, 1985. [CrossRef]
25. Stevens, A.J.; Clarke, D.; Nicholls, R.J.; Wadey, M.P. Estimating the Long-Term Historic Evolution of Exposure to Flooding of Coastal Populations. *Nat. Hazards Earth Syst. Sci.* **2015**, *15*, 1215–1229. [CrossRef]
26. Kraas, F. (Ed.) *Mega Cities, Mega Challenge: Informal Dynamics of Global Change: Insights from Dhaka, Bangladesh and Pearl River Delta, China*; Borntraeger Science Publishers: Stuttgart, Germany, 2019; ISBN 978-3-443-01103-1.
27. Tessler, Z.D.; Vörösmarty, C.J.; Grossberg, M.; Gladkova, I.; Aizenman, H.; Syvitski, J.P.M.; Foufoula-Georgiou, E. Profiling Risk and Sustainability in Coastal Deltas of the World. *Science* **2015**, *349*, 638–643. [CrossRef] [PubMed]
28. Shirzaei, M.; Freymueller, J.; Törnqvist, T.E.; Galloway, D.L.; Dura, T.; Minderhoud, P.S.J. Measuring, Modelling and Projecting Coastal Land Subsidence. *Nat. Rev. Earth Environ.* **2021**, *2*, 40–58. [CrossRef]
29. Minderhoud, P.S.J.; Coumou, L.; Erban, L.E.; Middelkoop, H.; Stouthamer, E.; Addink, E.A. The Relation between Land Use and Subsidence in the Vietnamese Mekong Delta. *Sci. Total Environ.* **2018**, *634*, 715–726. [CrossRef] [PubMed]
30. Giosan, L.; Naing, T.; Min Tun, M.; Clift, P.D.; Filip, F.; Constantinescu, S.; Khonde, N.; Blusztajn, J.; Buylaert, J.-P.; Stevens, T. On the Holocene Evolution of the Ayeyawady Megadelta. *Earth Surf. Dynam.* **2018**, *6*, 451–466. [CrossRef]
31. Anthony, E.J.; Besset, M.; Dussouillez, P.; Goichot, M.; Loisel, H. Overview of the Monsoon-Influenced Ayeyarwady River Delta, and Delta Shoreline Mobility in Response to Changing Fluvial Sediment Supply. *Mar. Geol.* **2019**, *417*, 106038. [CrossRef]
32. Latrubesse, E.M.; Park, E.; Kästner, K. The Ayeyarwady River (Myanmar): Washload Transport and Its Global Role among Rivers in the Anthropocene. *PLoS ONE* **2021**, *16*, e0251156. [CrossRef]
33. Adas, M. *The Burma Delta: Economic Development and Social Change on an Asian Rice Frontier, 1852–1941*; New Perspectives in Southeast Asian Studies; University of Wisconsin Press: Madison, WI, USA, 2011; ISBN 978-0-299-28354-4.
34. Heymann, J.; Löffler, E. Mangrove Degradation in the Ayeyarwady Delta, Myanmar. *Petermanns Geogr. Mitt.* **1997**, *141*, 291–306.
35. Lwin, N.N.; Zaw, K.; Nyein, K.T.; Thandar, M. Agricultural Transformation, Institutional Changes, and Rural Development in Ayeyarwady Delta, Myanmar. In *Agricultural Development, Trade & Regional Cooperation in Developing East Asia*; Intal, P.S., Jr., Oum, S., Simorangkir, M.J.O., Eds.; Economic Research Institute for ASEAN and East Asia (ERIA): Jakarta, Indonesia, 2011; pp. 307–355; ISBN 978-602-8660-43-3.
36. Webb, E.L.; Jachowski, N.R.A.; Phelps, J.; Friess, D.A.; Than, M.M.; Ziegler, A.D. Deforestation in the Ayeyarwady Delta and the Conservation Implications of an Internationally-Engaged Myanmar. *Glob. Environ. Chang.* **2014**, *24*, 321–333. [CrossRef]
37. Kraas, F. Ökonomische Transformationen im Delta des Ayeyarwady/Myanmar. *Geogr. Rundsch.* **2016**, *68*, 24–29.
38. Kuemmerle, T.; Erb, K.; Meyfroidt, P.; Müller, D.; Verburg, P.H.; Estel, S.; Haberl, H.; Hostert, P.; Jepsen, M.R.; Kastner, T. Challenges and Opportunities in Mapping Land Use Intensity Globally. *Curr. Opin. Environ. Sustain.* **2013**, *5*, 484–493. [CrossRef]
39. Wulder, M.A.; Coops, N.C.; Roy, D.P.; White, J.C.; Hermosilla, T. Land Cover 2.0. *Int. J. Remote Sens.* **2018**, *39*, 4254–4284. [CrossRef]
40. De Leeuw, J.; Georgiadou, Y.; Kerle, N.; Gier, A.; Inoue, Y.; Ferwerda, J.; Smies, M.; Narantuya, D. The Function of Remote Sensing in Support of Environmental Policy. *Remote Sens.* **2010**, *2*, 1731–1750. [CrossRef]
41. Kaku, K. Satellite Remote Sensing for Disaster Management Support: A Holistic and Staged Approach Based on Case Studies in Sentinel Asia. *Int. J. Disaster Risk Reduct.* **2019**, *33*, 417–432. [CrossRef]
42. Torbick, N.; Chowdhury, D.; Salas, W.; Qi, J. Monitoring Rice Agriculture across Myanmar Using Time Series Sentinel-1 Assisted by Landsat-8 and PALSAR-2. *Remote Sens.* **2017**, *9*, 119. [CrossRef]
43. Sakai, T.; Omori, K.; Oo, A.N.; Zaw, Y.N. Monitoring Saline Intrusion in the Ayeyarwady Delta, Myanmar, Using Data from the Sentinel-2 Satellite Mission. *Paddy Water Environ.* **2021**, *19*, 283–294. [CrossRef]
44. Khaing, S.S.; Aung, S.W.Y.; Aung, S.T. Analysis of Environmental Change Detection Using Satellite Images (Case Study: Irrawaddy Delta, Myanmar). In *Big Data Analysis and Deep Learning Applications*; Zin, T.T., Lin, J.C.-W., Eds.; Advances in Intelligent Systems and Computing; Springer: Singapore, 2019; Volume 744, pp. 355–363; ISBN 9789811308680.

45. Hedley, P.J.; Bird, M.I.; Robinson, R.A.J. Evolution of the Irrawaddy Delta Region since 1850: Evolution of the Irrawaddy Delta Region since 1850. *Geogr. J.* **2010**, *176*, 138–149. [CrossRef]
46. Chen, D.; Li, X.; Saito, Y.; Liu, J.P.; Duan, Y.; Liu, S.; Zhang, L. Recent Evolution of the Irrawaddy (Ayeyarwady) Delta and the Impacts of Anthropogenic Activities: A Review and Remote Sensing Survey. *Geomorphology* **2020**, *365*, 107231. [CrossRef]
47. Salmivaara, A.; Kummu, M.; Keskinen, M.; Varis, O. Using Global Datasets to Create Environmental Profiles for Data-Poor Regions: A Case from the Irrawaddy and Salween River Basins. *Environ. Manag.* **2013**, *51*, 897–911. [CrossRef] [PubMed]
48. De Alban, J.; Prescott, G.; Woods, K.; Jamaludin, J.; Latt, K.; Lim, C.; Maung, A.; Webb, E. Integrating Analytical Frameworks to Investigate Land-Cover Regime Shifts in Dynamic Landscapes. *Sustainability* **2019**, *11*, 1139. [CrossRef]
49. Quost, B.; Masson, M.-H.; Denœux, T. Classifier Fusion in the Dempster–Shafer Framework Using Optimized t-Norm Based Combination Rules. *Int. J. Approx. Reason.* **2011**, *52*, 353–374. [CrossRef]
50. Du, P.; Xia, J.; Zhang, W.; Tan, K.; Liu, Y.; Liu, S. Multiple Classifier System for Remote Sensing Image Classification: A Review. *Sensors* **2012**, *12*, 4764–4792. [CrossRef]
51. Nyi Nyi. *Articles on the Physiography of Burma*; Geological Society, Arts and Science University: Yangon, Myanmar, 1967.
52. Bender, F. *Geology of Burma*; Schweizerbart Science Publishers: Stuttgart, Germany, 1983; ISBN 978-3-443-11016-1.
53. Hla Tun Aung. *Myanmar, the Study of Processes and Patters*; National Centre for Human Resource Development, Publishing Committee, Ministry of Education: Yangon, Myanmar, 2003.
54. Kraas, F.; Spohner, R.; Aye Aye Myint. *Socio-Economic Atlas of Myanmar*; Franz Steiner: Stuttgart, Germany, 2017; ISBN 978-3-515-11625-1.
55. Robinson, R.A.J.; Bird, M.I.; Nay Win Oo; Hoey, T.B.; Maung Maung Aye; Higgitt, D.L.; Win, S.L. The Irrawaddy River Sediment Flux to the Indian Ocean: The Original Nineteenth-Century Data Revisited. *J. Geol.* **2007**, *115*, 629–640. [CrossRef]
56. Bird, M.I.; Robinson, R.A.J.; Nay Win Oo; Maung Maung Aye; Lu, X.X.; Higgitt, D.L.; Hoey, T.B. Preliminary Estimate of Organic Carbon Transport by the Ayeyarwady (Irrawaddy) and Thanlwin (Salween) Rivers of Myanmar. *Quat. Int.* **2008**, *186*, 113–122. [CrossRef]
57. Furuichi, T.; Win, Z.; Wasson, R.J. Discharge and Suspended Sediment Transport in the Ayeyarwady River, Myanmar: Centennial and Decadal Changes. *Hydrol. Process.* **2009**, *23*, 1631–1641. [CrossRef]
58. Fee, L.; Gibert, M.; Bartlett, R.; Capizzi, P.; Horton, R.; Lesk, C. *Climate Change Vulnerability Assessment of Labutta Township, Myanmar, 2016–2050: Scenarios for Building Resilience*; UN-Habitat-UN Environment: Nairobi, Kenya, 2017; p. 170.
59. Kraas, F.; Khin Khin Han. Climate: Temperature and Precipitation. In *Socio-Economic Atlas of Myanmar*; Kraas, F., Spohner, R., Aye Aye Myint, Eds.; Franz Steiner: Stuttgart, Germany, 2017; pp. 44–47; ISBN 978-3-515-11623-7.
60. Mie Sein, Z.M.; Ullah, I.; Saleem, F.; Zhi, X.; Syed, S.; Azam, K. Interdecadal Variability in Myanmar Rainfall in the Monsoon Season (May–October) Using Eigen Methods. *Water* **2021**, *13*, 729. [CrossRef]
61. Besset, M.; Anthony, E.J.; Dussouillez, P.; Goichot, M. The Impact of Cyclone Nargis on the Ayeyarwady (Irrawaddy) River Delta Shoreline and Nearshore Zone (Myanmar): Towards Degraded Delta Resilience? *Comptes Rendus Geosci.* **2017**, *349*, 238–247. [CrossRef]
62. Taft, L.; Evers, M. A Review of Current and Possible Future Human–Water Dynamics in Myanmar's River Basins. *Hydrol. Earth Syst. Sci.* **2016**, *20*, 4913–4928. [CrossRef]
63. Chhin, R.; Shwe, M.M.; Yoden, S. Time-lagged Correlations Associated with Interannual Variations of Pre-monsoon and Post-monsoon Precipitation in Myanmar and the Indochina Peninsula. *Int. J. Clim.* **2020**, *40*, 3792–3812. [CrossRef]
64. Nay Win Oo. Present State and Problems of Mangrove Management in Myanmar. *Trees* **2002**, *16*, 218–223. [CrossRef]
65. HIC. *Ayeyarwady State of the Basin Assessment (SOBA) 2017: Synthesis Report, Volume 1*; Hydro-Informatics Centre: Yangon, Myanmar, 2017; p. 251.
66. *The 2014 Myanmar Population and Housing Census. States and Region. Reports*; Ministry of Immigration and Population (MoIP): Nay Pyi Taw, Myanmar, 2015.
67. Kraas, F.; Gaese, H.; Mi Mi Kyi. *Megacity Yangon: Transformation Processes and Modern Developments, Second German-Myanmar Workshop in Yangon/Myanmar 2005*; LIT: Münster, Germany, 2006; Volume 7, ISBN 3-8258-0042-3.
68. Kraas, F.; Yin May; Zin Nwe Myint. Yangon/Myanmar: Transformation Processes and Mega-Urban Developments. *Geogr. Rundsch. Int.* **2010**, *6*, 26–37.
69. Kraas, F.; Aung Kyaw; Nay Win Oo. Agricultural Regions. In *Socio-Economic Atlas of Myanmar*; Kraas, F., Spohner, R., Aye Aye Myint, Eds.; Franz Steiner: Stuttgart, Germany, 2017; pp. 112–115; ISBN 978-3-515-11623-7.
70. Kraas, F.; Nilar Aung; Khin Khin Soe. Aquaculture. In *Socio-Economic Atlas of Myanmar*; Kraas, F., Spohner, R., Aye Aye Myint, Eds.; Franz Steiner Verlag: Stuttgart, Germany, 2017; pp. 118–121; ISBN 978-3-515-11623-7.
71. Khin Khin Soe. Climate Change Effects on Agriculture in Thabaung Township, Ayeyarwady Region, Myanmar: Challenges and Perceptions of Farmers. *IOP Conf. Ser. Earth Environ. Sci.* **2020**, *451*, 012030. [CrossRef]
72. Syvitski, J.P.M.; Kettner, A.J.; Overeem, I.; Hutton, E.W.H.; Hannon, M.T.; Brakenridge, G.R.; Day, J.; Vörösmarty, C.; Saito, Y.; Giosan, L. Sinking Deltas Due to Human Activities. *Nat. Geosci* **2009**, *2*, 681–686. [CrossRef]
73. Chaves, M.E.D.; Picoli, M.C.A.; Sanches, I.D. Recent Applications of Landsat 8/OLI and Sentinel-2/MSI for Land Use and Land Cover Mapping: A Systematic Review. *Remote Sens.* **2020**, *12*, 3062. [CrossRef]
74. Karakus, P.; Karabork, H. Effect Of Pansharpened Image On Some Of Pixel Based And Object Based Classification Accuracy. *Int. Arch. Photogramm. Remote Sens. Spat. Inf. Sci.* **2016**, *XLI-B7*, 235–239. [CrossRef]

75. Gilbertson, J.K.; Kemp, J.; van Niekerk, A. Effect of Pan-Sharpening Multi-Temporal Landsat 8 Imagery for Crop Type Differentiation Using Different Classification Techniques. *Comput. Electron. Agric.* **2017**, *134*, 151–159. [CrossRef]
76. Ottinger, M.; Kuenzer, C.; Liu, G.; Wang, S.; Dech, S. Monitoring Land Cover Dynamics in the Yellow River Delta from 1995 to 2010 Based on Landsat 5 TM. *Appl. Geogr.* **2013**, *44*, 53–68. [CrossRef]
77. Tucker, C.J. Red and Photographic Infrared Linear Combinations for Monitoring Vegetation. *Remote Sens. Environ.* **1979**, *8*, 127–150. [CrossRef]
78. Gao, B. NDWI—A Normalized Difference Water Index for Remote Sensing of Vegetation Liquid Water from Space. *Remote Sens. Environ.* **1996**, *58*, 257–266. [CrossRef]
79. Martín, M.P.; Gómez, I.; Chuvieco, E. Performance of a Burned-Area Index (BAIM) for Mapping Mediterranean Burned Scars from MODIS Data. In Proceedings of the 5th International Workshop on Remote Sensing and GIS Applications to Forest Fire Management: Fire Effects Assessment, Zaragoza, Spain, 16–18 June 2005; pp. 193–198.
80. Lacaux, J.P.; Tourre, Y.M.; Vignolles, C.; Ndione, J.A.; Lafaye, M. Classification of Ponds from High-Spatial Resolution Remote Sensing: Application to Rift Valley Fever Epidemics in Senegal. *Remote Sens. Environ.* **2007**, *106*, 66–74. [CrossRef]
81. Gupta, K.; Mukhopadhyay, A.; Giri, S.; Chanda, A.; Majumdar, D.S.; Samanta, S.; Mitra, D.; Samal, R.N.; Pattnaik, A.K.; Hazra, S. An Index for Discrimination of Mangroves from Non-Mangroves Using LANDSAT 8 OLI Imagery. *MethodsX* **2018**, *5*, 1129–1139. [CrossRef]
82. Yancho, J.; Jones, T.; Gandhi, S.; Ferster, C.; Lin, A.; Glass, L. The Google Earth Engine Mangrove Mapping Methodology (GEEMMM). *Remote Sens.* **2020**, *12*, 3758. [CrossRef]
83. Haralick, R.M.; Shanmugam, K.; Dinstein, I. Textural Features for Image Classification. *IEEE Trans. Syst. Man Cybern.* **1973**, *SMC-3*, 610–621. [CrossRef]
84. Chatziantoniou, A.; Psomiadis, E.; Petropoulos, G. Co-Orbital Sentinel 1 and 2 for LULC Mapping with Emphasis on Wetlands in a Mediterranean Setting Based on Machine Learning. *Remote Sens.* **2017**, *9*, 1259. [CrossRef]
85. Belgiu, M.; Drăguţ, L. Random Forest in Remote Sensing: A Review of Applications and Future Directions. *ISPRS J. Photogramm. Remote Sens.* **2016**, *114*, 24–31. [CrossRef]
86. Breiman, L. Random Forests. *Mach. Learn.* **2001**, *45*, 5–32. [CrossRef]
87. Pal, M.; Mather, P.M. An Assessment of the Effectiveness of Decision Tree Methods for Land Cover Classification. *Remote Sens. Environ.* **2003**, *86*, 554–565. [CrossRef]
88. Maxwell, A.E.; Warner, T.A.; Fang, F. Implementation of Machine-Learning Classification in Remote Sensing: An Applied Review. *Int. J. Remote Sens.* **2018**, *39*, 2784–2817. [CrossRef]
89. Mountrakis, G.; Im, J.; Ogole, C. Support Vector Machines in Remote Sensing: A Review. *ISPRS J. Photogramm. Remote Sens.* **2011**, *66*, 247–259. [CrossRef]
90. Talukdar, S.; Singha, P.; Mahato, S.; Pal, S.; Liou, Y.A.; Rahman, A. Land-Use Land-Cover Classification by Machine Learning Classifiers for Satellite Observations—A Review. *Remote Sens.* **2020**, *12*, 1135. [CrossRef]
91. Meng, Q.; Cieszewski, C.J.; Madden, M.; Borders, B.E. K Nearest Neighbor Method for Forest Inventory Using Remote Sensing Data. *GIScience Remote Sens.* **2007**, *44*, 149–165. [CrossRef]
92. Yager, R.R. An Extension of the Naive Bayesian Classifier. *Inf. Sci.* **2006**, *176*, 577–588. [CrossRef]
93. Orfeo ToolBox (OTB) FusionOfClassifications—Orfeo ToolBox 8.0.1 Documentation. Available online: https://www.orfeotoolbox.org/CookBook/Applications/app_FusionOfClassifications.html (accessed on 12 June 2022).
94. Foody, G.M. Status of Land Cover Classification Accuracy Assessment. *Remote Sens. Environ.* **2002**, *80*, 185–201. [CrossRef]
95. Aldwaik, S.Z.; Pontius, R.G. Intensity Analysis to Unify Measurements of Size and Stationarity of Land Changes by Interval, Category, and Transition. *Landsc. Urban. Plan.* **2012**, *106*, 103–114. [CrossRef]
96. Fritz, H.M.; Blount, C.D.; Thwin, S.; Thu, M.K.; Chan, N. Cyclone Nargis Storm Surge in Myanmar. *Nat. Geosci* **2009**, *2*, 448–449. [CrossRef]
97. Renaud, F.G.; Syvitski, J.P.; Sebesvari, Z.; Werners, S.E.; Kremer, H.; Kuenzer, C.; Ramesh, R.; Jeuken, A.; Friedrich, J. Tipping from the Holocene to the Anthropocene: How Threatened Are Major World Deltas? *Curr. Opin. Environ. Sustain.* **2013**, *5*, 644–654. [CrossRef]
98. Radford, S.; Lamb, V. Work and Struggle of Fishing Livelihoods in the Delta: Development and 'New' Change along the Ayeyarwady (Irrawaddy) River, Myanmar. *Asia Pac. Viewp.* **2020**, *61*, 338–352. [CrossRef]
99. Dunn, F.E.; Minderhoud, P.S.J. Sedimentation Strategies Provide Effective but Limited Mitigation of Relative Sea-Level Rise in the Mekong Delta. *Commun. Earth Environ.* **2022**, *3*, 2. [CrossRef]
100. Horst, T.; Rutten, M.M.; Giesen, N.C.; Hanssen, R.F. Monitoring Land Subsidence in Yangon, Myanmar Using Sentinel-1 Persistent Scatterer Interferometry and Assessment of Driving Mechanisms. *Remote Sens. Environ.* **2018**, *217*, 101–110. [CrossRef]
101. Sakai, T.; Omori, K.; Oo, A.N.; Ma, S.S.; Zaw, Y.N. Decadal Changes in the Rice-Cropping System in the Ayeyarwady Delta Using a Large Archive of Satellite Imagery from 1981 to 2020. *Paddy Water Environ.* **2021**, *19*, 295–306. [CrossRef]
102. International Bank for Reconstruction and Development (IBRD). *Appraisal of Irrigation I Project Burma*; Irrigation and Area Development I Division Asia Projects Department: Washington, DC, USA, 1974; p. 142.
103. World Bank Group Archives. *Burma-Lower Burma Paddyland Development Project-Project Completion Repor-July 1986*; World Bank Group Archives: Washington, DC, USA, 1986; p. 75.

104. Ivars, B.; Venot, J.-P. Grounded and Global: Water Infrastructure Development and Policymaking in the Ayeyarwady Delta, Myanmar. *Water Altern.* **2019**, *12*, 1038–1063.
105. Schneider, P.; Asch, F. Rice Production and Food Security in Asian Mega Deltas—A Review on Characteristics, Vulnerabilities and Agricultural Adaptation Options to Cope with Climate Change. *J. Agro Crop. Sci* **2020**, *206*, 491–503. [CrossRef]
106. Seinn Seinn, M.U.; Ahmad, M.M.; Thapa, G.B.; Shrestha, R.P. Farmers' Adaptation to Rainfall Variability and Salinity through Agronomic Practices in Lower Ayeyarwady Delta, Myanmar. *J. Earth Sci. Clim. Chang.* **2015**, *6*, 1. [CrossRef]
107. Lar, N.M.; Arunrat, N.; Tint, S.; Pumijumnong, N. Assessment of the Potential Climate Change on Rice Yield in Lower Ayeyarwady Delta of Myanmar Using EPIC Model. *Environ. Nat. Resour. J.* **2018**, *16*, 45–57. [CrossRef]
108. Kattelus, M.; Rahaman, M.M.; Varis, O. Myanmar under Reform: Emerging Pressures on Water, Energy and Food Security. *Nat. Resour. Forum.* **2014**, *38*, 85–98. [CrossRef]
109. Pörtner, H.-O.; Roberts, D.C.; Tignor, M.; Poloczanska, E.S.; Mintenbeck, K.; Alegría, A.; Craig, M.; Langsdorf, S.; Löschke, S.; Möller, V.; et al. (Eds.) *IPCC, 2022: Climate Change 2022: Impacts, Adaptation, and Vulnerability. Contribution of Working Group II to the Sixth Assessment Report of the Intergovernmental Panel on Climate Change*; Cambridge University Press: Cambridge, UK, 2022; *in press*.
110. Yang, R.; Luo, Y.; Yang, K.; Hong, L.; Zhou, X. Analysis of Forest Deforestation and Its Driving Factors in Myanmar from 1988 to 2017. *Sustainability* **2019**, *11*, 3047. [CrossRef]
111. Zin Nwe Myint. Woodfuel Uses: A Distinct Phenomenon in Megacity Yangon, Myanmar. In *Megacity Yangon: Transformation Processes and Modern Developments*; Southeast Asian Modernities; Kraas, F., Gaese, H., Mi Mi Kyi, Eds.; Lit Publishers: Berlin, Germany, 2006; Volume 7, pp. 261–284.
112. Kuenzer, C.; Bluemel, A.; Gebhardt, S.; Quoc, T.V.; Dech, S. Remote Sensing of Mangrove Ecosystems: A Review. *Remote Sens.* **2011**, *3*, 878–928. [CrossRef]
113. Veettil, B.K.; Pereira, S.F.R.; Quang, N.X. Rapidly Diminishing Mangrove Forests in Myanmar (Burma): A Review. *Hydrobiologia* **2018**, *822*, 19–35. [CrossRef]
114. Beveridge, M.C.M.; Little, D.C. The History of Aquaculture in Traditional Societies. In *Ecological Aquaculture*; Costa-Pierce, B.A., Ed.; Blackwell Science Ltd.: Oxford, UK, 2002; pp. 1–29; ISBN 978-0-470-99505-1.
115. Belton, B.; Hein, A.; Htoo, K.; Kham, L.S.; Nischan, U.; Reardon, T.; Boughton, D. *Aquaculture in Transition: Value Chain Transformation, Fish and Food Security in Myanmar*; Feed the Future Innovation Lab for Food Security Policy Research Paper 8; Michigan State University: East Lansing, MI, USA, 2015.
116. Higgins, S.; Overeem, I.; Tanaka, A.; Syvitski, J.P.M. Land Subsidence at Aquaculture Facilities in the Yellow River Delta, China. *Geophys. Res. Lett.* **2013**, *40*, 3898–3902. [CrossRef]
117. Hung, W.-C.; Hwang, C.; Chen, Y.-A.; Zhang, L.; Chen, K.-H.; Wei, S.-H.; Huang, D.-R.; Lin, S.-H. Land Subsidence in Chiayi, Taiwan, from Compaction Well, Leveling and ALOS/PALSAR: Aquaculture-Induced Relative Sea Level Rise. *Remote Sens.* **2017**, *10*, 40. [CrossRef]
118. Liu, S.; Li, X.; Chen, D.; Duan, Y.; Ji, H.; Zhang, L.; Chai, Q.; Hu, X. Understanding Land Use/Land Cover Dynamics and Impacts of Human Activities in the Mekong Delta over the Last 40 Years. *Glob. Ecol. Conserv.* **2020**, *22*, e00991. [CrossRef]
119. Kuenzer, C.; van Beijma, S.; Gessner, U.; Dech, S. Land Surface Dynamics and Environmental Challenges of the Niger Delta, Africa: Remote Sensing-Based Analyses Spanning Three Decades (1986–2013). *Appl. Geogr.* **2014**, *53*, 354–368. [CrossRef]
120. Nababa, I.; Symeonakis, E.; Koukoulas, S.; Higginbottom, T.; Cavan, G.; Marsden, S. Land Cover Dynamics and Mangrove Degradation in the Niger Delta Region. *Remote Sens.* **2020**, *12*, 3619. [CrossRef]
121. Ottinger, M.; Clauss, K.; Kuenzer, C. Large-Scale Assessment of Coastal Aquaculture Ponds with Sentinel-1 Time Series Data. *Remote Sens.* **2017**, *9*, 440. [CrossRef]
122. Elhag, M.; Gitas, I.; Othman, A.; Bahrawi, J. Effect of Water Surface Area on the Remotely Sensed Water Quality Parameters of Baysh Dam Lake, Saudi Arabia. *Hydrol. Earth Syst. Sci. Discuss.* **2019**, *2019*, 1–20. [CrossRef]
123. Ottinger, M.; Bachofer, F.; Huth, J.; Kuenzer, C. Mapping Aquaculture Ponds for the Coastal Zone of Asia with Sentinel-1 and Sentinel-2 Time Series. *Remote Sens.* **2021**, *14*, 153. [CrossRef]
124. Ma, L.; Li, M.; Ma, X.; Cheng, L.; Du, P.; Liu, Y. A Review of Supervised Object-Based Land-Cover Image Classification. *ISPRS J. Photogramm. Remote Sens.* **2017**, *130*, 277–293. [CrossRef]